The Adaptable 4A Inversion (5AI): Description and first XCO_2 retrievals from OCO-2 observations

Matthieu Dogniaux[1], Cyril Crevoisier[1], Raymond Armante[1], Virginie Capelle[1], Thibault Delahaye[1], Vincent Cassé[1], Martine De Mazière[2], Nicholas M. Deutscher[3,4], Dietrich G. Feist[5,6,7], Omaira E. Garcia[8], David W. T. Griffith[3], Frank Hase[9], Laura T. Iraci[10], Rigel Kivi[11], Isamu Morino[12], Justus Notholt[4], David F. Pollard[13], Coleen M. Roehl[14], Kei Shiomi[15], Kimberly Strong[16], Yao Té[17], Voltaire A. Velazco[3], Thorsten Warneke[4]

[1]Laboratoire de Météorologie Dynamique/IPSL, CNRS, École polytechnique, Institut Polytechnique de Paris, Sorbonne Université, École Normale Supérieure, PSL Research University, Palaiseau, 91120, France
[2]Royal Belgian Institute for Space Aeronomy, Brussels, Belgium
[3]Centre for Atmospheric Chemistry, School of Earth, Atmospheric and Life Sciences, University of Wollongong, Wollongong, Australia
[4]University of Bremen, Bremen, Germany
[5]Max Planck Institute for Biogeochemistry, Jena, Germany
[6]Ludwig-Maximilians-Universität München, Lehrstuhl für Physik der Atmosphäre, Munich, Germany
[7]Deutsches Zentrum für Luft- und Raumfahrt, Institut für Physik der Atmosphäre, Oberpfaffenhofen, Germany
[8]Izaña Atmospheric Research Center (IARC), State Meteorological Agency of Spain (AEMET), Spain
[9]Karlsruhe Institute of Technology (KIT), Institute of Meteorology and Climate Research (IMK-ASF), Karlsruhe, Germany
[10]NASA Ames Research Center, Moffett Field, CA, USA
[11]Finnish Meteorological Institute, Sodankylä, Finland
[12]National Institute for Environmental Studies (NIES), Tsukuba, Japan
[13]National Institute of Water and Atmospheric Research Ltd (NIWA), Lauder, New Zealand
[14]Division of Geological and Planetary Sciences, California Institute of Technology, Pasadena, CA, USA
[15]Japan Aerospace Exploration Agency (JAXA), Tsukuba, Japan
[16]Department of Physics, University of Toronto, Toronto, Canada
[17]Laboratoire d'Etudes du Rayonnement et de la Matière en Astrophysique et Atmosphères (LERMA-IPSL), Sorbonne Université, CNRS, Observatoire de Paris, PSL Université, 75005 Paris, France

Correspondence to: Matthieu Dogniaux (matthieu.dogniaux@lmd.ipsl.fr)

Abstract. A better understanding of greenhouse gas surface sources and sinks is required in order to address the global challenge of climate change. Spaceborne remote estimations of greenhouse gas atmospheric concentrations can offer the global coverage that is necessary to improve the constraint on their fluxes, thus enabling a better monitoring of anthropogenic emissions. In this work, we introduce the Adaptable 4A Inversion (5AI) inverse scheme that aims to retrieve geophysical parameters from any remote sensing observation. The algorithm is based on the Optimal Estimation algorithm, relying on the Operational version of the Automatized Atmospheric Absorption Atlas (4A/OP) radiative transfer forward model along with the Gestion et Étude des Informations Spectroscopiques Atmosphériques: Management and Study of Atmospheric Spectroscopic Information (GEISA) spectroscopic database. Here, the 5AI scheme is applied to retrieve the column-averaged dry-air mole fraction of carbon dioxide (X_{CO_2}) from a sample of measurements performed by the Orbiting Carbon Observatory-2 (OCO-2) mission. Those have been selected as a compromise between coverage and the lowest

aerosol content possible, so that the impact of scattering particles can be neglected, for computational time purposes. For airmasses below 3.0, 5AI X_{CO_2} retrievals successfully capture the latitudinal variations of CO_2, as well as its seasonal cycle and long-term increasing trend. Comparison with ground-based observations from the Total Carbon Column Observing Network (TCCON) yields a bias of 1.30 ± 1.32 ppm, which is comparable to the standard deviation of the Atmospheric CO_2 Observations from Space (ACOS) official products over the same set of soundings. These non-scattering 5AI results however exhibit an average difference of about 3 ppm with regard to ACOS results. We show that neglecting scattering particles for computational time purposes can explain most of this difference that can be fully corrected by adding to OCO-2 measurements an average 'calculated – observed' spectral residual correction, which encompasses all the inverse setup and forward differences between 5AI and ACOS. These comparisons show the reliability of 5AI as an Optimal Estimation implementation that is easily adaptable to any instrument designed to retrieve column-averaged dry-air mole fractions of greenhouse gases.

1. Introduction

The atmospheric concentration of carbon dioxide (CO_2) has been rising for decades because of fossil fuel emissions as well as land-use changes. However, large uncertainties still remain in the global carbon budget (e.g. Le Quéré et al., 2009). In order to address the global challenge of climate change, a better understanding of carbon sources and sinks is necessary and remote spaceborne estimations of CO_2 columns can help constraining these carbon fluxes in atmospheric inversion studies, and thus reducing the remaining uncertainties (e.g. Rayner and O'Brien, 2001; Chevallier et al., 2007; Basu et al., 2013, 2018).

The column-averaged dry-air mole fraction of CO_2 (X_{CO_2}) can be retrieved from thermal infrared (TIR) soundings, mostly sensitive to the mid-troposphere (e.g. Chédin et al., 2003; Crevoisier et al., 2004, 2009a), as well as from near-infrared (NIR) and shortwave infrared (SWIR) measurements, which are sensitive to the whole atmospheric column, and especially to levels close to the surface, where carbon fluxes take place. Current NIR and SWIR satellite missions observing carbon dioxide include the Japanese Greenhouse gases Observing SATellites (GOSAT and GOSAT-2), NASA's Orbiting Carbon Observatory-2 and 3 (OCO-2 and OCO-3) and the Chinese mission TanSat. Over time, different algorithms have been developed to exploit their measurements: those rely on different inverse methods and use various hypotheses to address the fundamentally ill-posed problem of X_{CO_2} retrieval. These algorithms notably include the Japanese National Institute for Environmental Studies (NIES) algorithm (Yokota et al., 2009; Yoshida et al., 2011, 2013), as well as the Atmospheric CO_2 Observations from Space (ACOS) algorithm (Bösch et al., 2006; Connor et al., 2008; O'Dell et al., 2012, 2018), UoL-FP from the University of Leicester (Parker et al., 2011), RemoTeC from the Netherlands Institute for Space Research (SRON) (Butz et al., 2011; Wu et al., 2018) and the Fast atmOspheric traCe gAs retrievaL (FOCAL) algorithm from the University of Bremen (Reuter et al., 2017a, 2017b).

They also rely on different forward radiative transfer models to compute synthetic measurements and their partial derivatives. It was noted, for the Scanning Imaging Absorption Spectrometer for Atmospheric Chartography (SCIAMACHY) mission (Bovensmann et al., 1999), that NIR and SWIR measurements are also quite sensitive to the presence of scattering particles on the optical path, which can then substantially perturb X_{CO_2} retrievals if unaccounted for (Houweling et al., 2005). As exact multiple scattering calculations are too time-expensive for operational X_{CO_2} retrievals, all the previously mentioned retrieval algorithms have radiative transfer models that implement various approximations to speed-up forward modelling. Finally, radiative transfer fundamentally depends on spectroscopic databases that contain the parameters enabling to compute atmospheric gas absorption. The HITRAN spectroscopic database (latest version 2016: Gordon et al., 2017) is widely used for greenhouse gas concentration retrievals, as are the ABSCO atmospheric absorption tables for the ACOS algorithm (Drouin et al., 2017; Oyafuso et al., 2017).

The design of an X_{CO_2} retrieval algorithm, from the forward model and the spectroscopic parameters it uses to the choice of the adjusted quantities in the state vector, has a critical influence on the overall performance of the observing system (Rodgers, 2000). The systematic errors in retrieved X_{CO_2} and their standard deviations (the latter being also called single measurement precision) with regard to the true (but unknown) state of the atmosphere particularly impact the uncertainty reduction and bias in atmospheric CO_2 flux inversion studies (e.g. Chevallier et al., 2007). Retrieved X_{CO_2} products are most often validated against columns with similar observation geometry, like the ground based solar absorption spectrometry. The Total Carbon Column Observing Network (TCCON) is a network of ground stations that retrieve column-averaged dry-air mole fraction of CO_2 and other species from NIR and SWIR spectra measured with Fourier Transform Spectrometers (FTS) directly pointing at the sun (Wunch et al., 2011b). The network currently consists of 27 stations all around the world and its products constitute a "truth-proxy" reference for the validation of spaceborne retrievals of greenhouse gas atmospheric concentrations. For instance, TCCON datasets were used to validate SCIAMACHY (Reuter et al., 2011), GOSAT X_{CO_2} retrieved by the ACOS (Wunch et al., 2011a) and NIES algorithms (Inoue et al., 2016) and OCO-2 X_{CO_2} produced by ACOS (O'Dell et al., 2018; Wunch et al., 2017), RemoTeC (Wu et al., 2018) and FOCAL (Reuter et al., 2017b). These three last algorithms exhibit different biases with regard to TCCON, depending on their respective forward modelling and bias correction strategies: 0.30 ± 1.04 ppm, 0.0 ± 1.36 ppm and 0.67 ± 1.34 ppm for OCO-2 nadir land soundings, respectively.

In this paper, we present the Adaptable 4A Inversion (5AI) that implements the Optimal Estimation inverse method (Rodgers, 2000). 5AI relies on the OPerational version of the Automatized Atmospheric Absorption Atlas (4A/OP) radiative transfer model (Scott and Chédin, 1981; Tournier, 1995; Cheruy et al., 1995) (https://4aop.aeris-data.fr) and the GEISA (Gestion et Étude des Informations Spectroscopiques Atmosphériques: Management and Study of Spectroscopic Information) spectroscopic database (Jacquinet-Husson et al., 2016) (http://cds-espri.ipsl.fr/etherTypo/?id=950). The 5AI

scheme is applied to retrieve X_{CO_2} from a sample of OCO-2 measurements that compromises between coverage and the lowest possible values of ACOS retrieved aerosol optical depth in order to avoid possible singular biases due to strong aerosol events. This sample selection comprises: (1) OCO-2 best flag target mode soundings between 2014 and 2018 and (2) a sample of two years of OCO-2 nadir measurements with a global land coverage. First, for computational time purposes, retrievals are performed without taking into account scattering particles. We then discuss how considering them and accounting for differences in the radiative transfer modelling and retrieval setups impact the 5AI results, which are compared to ACOS and TCCON reference data over identical sets of soundings.

This paper is organized as follows: Sect. 2 describes the 5AI retrieval scheme and its current features, as well as the 4A/OP radiative transfer model, the GEISA spectroscopic database and the empirically corrected O_2 A-band absorption continuum on which it relies. Section 3 presents the OCO-2 and TCCON data selection. Section 4 presents the a posteriori filters used for this work and shows the 5AI X_{CO_2} target and nadir retrieval results which are compared to TCCON and ACOS (B8r version). 5AI results are discussed in Sect. 5. It shows how taking into account scattering particles in 5AI retrievals can impact the results, as well as how systematic differences between different X_{CO_2} products can be accounted for by compensating them with a spectral residual adjustment. Section 6 finally highlights the conclusions of this work.

2. The 5AI retrieval scheme

As for any other retrieval scheme, 5AI aims at finding the estimate of atmospheric and surface parameters (for example trace gas concentration, temperature profile, surface albedo, or scattering particle optical depth) that best fits hyperspectral measurements made from space. This inverse problem can be expressed with the following equation:

$$\boldsymbol{y} = \boldsymbol{F}(\boldsymbol{x}) + \boldsymbol{\varepsilon} \qquad\qquad (1)$$

where $\boldsymbol{y}$ is the measurement vector containing the radiances measured by the space instrument, $\boldsymbol{x}$ is the state vector containing the geophysical parameters to be retrieved, $\boldsymbol{\varepsilon}$ is the measurement noise and finally $\boldsymbol{F}$ is the forward radiative transfer model that describes the physics linking the geophysical parameters to be retrieved to the measured infrared radiances.

2.1 Forward modelling: 4A/OP and GEISA spectroscopic database

The 5AI retrieval scheme uses the OPerational version of the Automatized Atmospheric Absorption Atlas (4A/OP). 4A/OP is an accurate line-by-line radiative transfer model that enables a fast computation of atmospheric transmittances based on atlases containing pre-computed monochromatic optical thicknesses for reference atmospheres. Those are used to compute atmospheric transmittances, for any input atmospheric profile and viewing configuration, that enable to solve the radiative transfer equation and yield radiances and their partial derivatives with regard to the input geophysical parameters at a pseudo-infinite spectral resolution (0.0005 cm^{-1} best) or convolved with an instrument function. 4A/OP is the reference

radiative transfer model for the Centre National d'Études Spatiales (CNES) IASI Level 1 Calibration/Validation and operational processing, and it is used for daily retrieval of mid-tropospheric columns of CO_2 (Crevoisier et al., 2009a) and CH_4 (Crevoisier et al., 2009b) from the Infrared Atmospheric Sounding Imager (IASI). Moreover, 4A/OP has also been chosen by CNES as the reference radiative transfer model for the development of the New Generation of the IASI instrument (IASI-NG) (Crevoisier et al., 2014), as well as the French NIR and SWIR CO_2 remote sensing MicroCarb mission (Pascal et al., 2017) and the French-German MEthane Remote sensing LIdar Mission (MERLIN) (Ehret et al., 2017).

Although originally developed for the thermal infrared spectral region, 4A/OP has been extended to the near and shortwave infrared regions (NIR and SWIR): (1) The computation of the atlases of optical thickness was extended to the 3,000 – 13,500 cm^{-1} domain and takes into account line-mixing and collision-induced absorption (CIA) in the O_2 A-band (Tran and Hartmann, 2008) as well as line-mixing and H_2O-broadening of CO_2 lines (Lamouroux et al., 2010). The absorption lines of CO_2 we use in this work are thus identical to those included in HITRAN 2008; (2) Solar spectrum is a flexible input and the Doppler shift of its lines is computed; (3) The radiative transfer model is now coupled with the LIDORT model (Spurr, 2002) for scalar multiple-scattering simulation performed with the discrete ordinates method, as well as with VLIDORT (Spurr, 2006) if polarization or Bidirectional Reflectance Distribution Functions (BRDF) need to be taken into account. This coupling especially enables to take into account Rayleigh scattering and if necessary scattering particles in NIR and SWIR forward modelling.

The 4A/OP radiative transfer model can be used with monochromatic optical thickness atlases computed from any spectroscopic database. For this present work, the atlases are computed using the GEISA 2015 (Gestion et Étude des Informations Spectroscopiques Atmosphériques: Management and Study of Spectroscopic Information) spectroscopic database. Being the base of many projects since the beginning in the astronomical and astrophysical communities, GEISA has also been used since the 2000's for the preparation of several current and future spatial missions, and has been chosen by CNES as the reference spectroscopic database for the definition of IASI-NG, MicroCarb and MERLIN. Due to imperfections in the Tran and Hartmann (2008) line mixing and CIA models, an empirical correction to the absorption continuum in the O_2 A-band, fitted from Park Falls TCCON spectra following the method described in Drouin et al. (2017), has been added. Finally, we use Toon (2015) as input solar spectra.

2.2 Inverse modelling in the 5AI retrieval scheme

2.2.1 Optimal estimation applied for X_{CO_2} retrieval

The whole formalism of Optimal Estimation that enables to find a satisfying solution to Eq. (1) may be found in Rodgers (2000). This subsection only outlines the key steps that are implemented in order to retrieve X_{CO_2}.

Equation (1) includes $\boldsymbol{\varepsilon}$, the experimental noise of the measured radiances. Hence, it appears more appropriate to use a formalism that takes into account this measurement uncertainty and translates it into retrieval uncertainty: this is done by representing the state of the atmosphere $\boldsymbol{x}$ and the measurement $\boldsymbol{y}$ as random variables. Assuming Gaussian statistics, the inversion problem consists in finding the state vector which compromises between an *a priori* knowledge of the geophysical state parameters (most often brought by climatologies) and the information brought by the measurement, both weighted by their respective uncertainties. It finally boils down to the minimization of the following χ^2 cost function:

$$\chi^2 = \left(y - F(x)\right)^T S_e^{-1}\left(y - F(x)\right) + (x - x_a)^T S_a^{-1}(x - x_a) \tag{2}$$

where $\boldsymbol{x_a}$ is the *a priori* state vector, which is also in most cases chosen as the first guess for iterative retrievals. Assuming again Gaussian statistics, $\boldsymbol{S_a}$ is the *a priori* state covariance matrix that represents the variability around the *a priori* state vector, and similarly $\boldsymbol{S_e}$ is the *a priori* measurement error covariance matrix that represents the noise model of the instrument. Moreover, as the forward model for this retrieval is highly non-linear, it is practical to use a local linear approximation, here expressed around the *a priori* state:

$$F(x) = F(x_a) + \frac{\partial F}{\partial x}\big|_{x_a}(x - x_a) \quad . \tag{3}$$

The partial derivatives of the forward radiative transfer model $\boldsymbol{F}$ (here 4A/OP) are expressed as a matrix, called the Jacobian matrix, and denoted $\boldsymbol{K}$.

All these assumptions enable the maximum posterior probability state $\widehat{x}$ that minimizes the cost function defined in Eq. (2) to be found. It can be computed by iteration, using the general approach:

$$x_{i+1} = x_i + \left[(1 + \gamma)S_a^{-1} + K_i^T S_e^{-1} K_i\right]^{-1}\left(K_i^T S_e^{-1}\left(y - F(x_i)\right) - S_a^{-1}(x_i - x_a)\right) \tag{4}$$

where γ is a scaling factor that can be set to 0 (Gauss-Newton method) or whose value can be adapted along iterations in order to prevent divergence (Levenberg-Marquardt method, in which successful retrievals use decreasing γ values and eventually 0 for the final iteration). $\boldsymbol{K_i}$ denotes here the forward radiative transfer Jacobian matrix, whose values are evaluated for the state vector $\boldsymbol{x_i}$.

A successful retrieval reduces the *a priori* uncertainty of the state vector described in $\boldsymbol{S_a}$. The *a posteriori* covariance matrix of the retrieved state vector $\widehat{\boldsymbol{S}}$, whose diagonal elements give the posterior variance of the retrieved state vector elements, is expressed as

$$\widehat{S} = [S_a^{-1} + K^T S_e^{-1} K]^{-1} \quad . \tag{5}$$

Finally, the sensitivity of the retrieval with regard to the true geophysical state $\boldsymbol{x_{true}}$ is given by the averaging kernel matrix $\boldsymbol{A}$ calculated according to

$$A = \frac{\partial \widehat{x}}{\partial x_{true}}(x_a) = [S_a^{-1} + K^T S_e^{-1} K]^{-1} K^T S_e^{-1} K \quad . \tag{6}$$

In most cases, the CO_2 concentration is included in the state vector as a level or layer profile from which X_{CO_2}, the retrieved column-averaged dry-air mole fraction of CO_2, is computed (e.g. O'Dell et al., 2012). If we note $\hat{x}_{CO2}$, the part of the retrieved state vector $\hat{x}$ containing the CO_2 profile, and A_{CO2} and $\hat{S}_{CO2}$, the corresponding square parts of A and $\hat{S}$, we have:

$$X_{CO_2} = h.\hat{x}_{CO2} \tag{7}$$

$$\sigma_{X_{CO_2}} = \sqrt{h^T \hat{S}_{CO_2} h} \tag{8}$$

$$\left(a_{CO2}\right)_j = \frac{\partial X_{CO_2}}{\partial x_{true}} = \frac{\left(h^T A_{CO2}\right)_j}{h_j} \tag{9}$$

where h is the pressure weighting function. $\sigma_{X_{CO_2}}$ denotes the posterior uncertainty of the retrieved X_{CO_2} and a_{CO2} is the CO_2 column averaging kernel. This profile vector describes the vertical sensitivity of the retrieved column with regard to the true profile: it is essential to characterize retrieval results and to compare them to other products, as shown in Sect. 4.2.

2.2.2 5AI features and retrieval scheme setups for OCO-2

The 5AI retrieval scheme enables the retrieval of multiple geophysical variables from hyperspectral measurements. Those currently include trace gas concentration represented in the state vector as a concentration profile or a profile scaling-factor, global temperature profile offset, surface temperature and pressure, band-wise albedo whose spectral dependence is modelled as a polynomial, and finally scattering particle layer-wise optical depth. For this work, the state vector includes the main geophysical parameters necessary to retrieve X_{CO_2} and is described in Table 1. The *a priori* values and their covariance are identical to those used in the ACOS B8r version (O'Dell et al., 2018) in order to ease the retrieval result comparison.

Table 1. 5AI state vector composition for OCO-2 retrievals

Variable name	Length	A priori value	A priori uncertainty (1σ)	Notes
H_2O scaling factor	1	1.0	0.5 (same as ACOS)	-
CO_2 layer concentration	19 layers	ACOS a priori	ACOS prior covariance matrix	See prior covariance matrix in (O'Dell et al., 2012)
Surface Pressure	1	ACOS a priori	4.0 hPa (same as ACOS)	-
Temperature profile offset	1	ACOS a priori	5.0 K (same as ACOS)	-
Surface Albedo (order 0 of albedo model)	3 bands	ACOS a priori	1.0 (same as ACOS)	Evaluated at 0.77, 1.615 and 2.06 μm for O_2, CO_2 weak and strong bands, respectively
Surface Albedo Slope (order 1 of albedo model)	3 bands	0.0	1.0 /cm^{-1}	-

The OCO-2 spectrometer measures Earth-reflected near and shortwave infrared (NIR and SWIR) sunlight in three distinct bands: the O_2 A-band (0.7 μm), the weak CO_2 band (1.6 μm) and the strong CO_2 band (2.0 μm). In order to accurately model OCO-2 measurements, polarization effects have to be taken into account. As 4A/OP coupling with (V)LIDORT is not optimal yet, forward calculations can reach unmanageable durations without some assumptions that allow faster radiative transfer simulations. Therefore, as explained in Sect. 1, we first restrict this work to the lowest scattering particle content possible (while compromising with coverage) so that only Rayleigh scattering needs to be taken into account in the O_2 A-band (0.7 μm). This is done by using 4A/OP coupling with VLIDORT, and the ACOS Stokes coefficients are applied to yield the final scalar radiances. For CO_2 weak and strong bands, scattering and polarization can be neglected with this low scattering particle content assumption, and only the Stokes coefficient 0.5 for the *I* component of the electric field is applied to yield the final scalar radiances. As we neglect, for computation time purposes, the possible impact of scattering particles in forward calculations and in the state vector, the retrieval problem becomes more linear. Thus we can also assume a slow variation of the Jacobian matrix along the retrieval iterations and therefore choose not to update it in order to save computational time. Hence, the partial derivatives of the radiative transfer model are evaluated once and for all around the *a priori* state. We performed a sensitivity test and assessed that this approximation does not significantly change the retrieval results (not shown).

3. Data

3.1 Data description

The OCO-2 satellite has three distinct observation modes. The nadir and glint modes are the nominal science observation modes; they constitute the vast majority of OCO-2 measurements. In addition, the target mode of the OCO-2 mission provides data for the validation of the retrievals. In target mode, the satellite tilts and aims at a validation target (most of them are TCCON stations) and scans its whereabouts several times during the overpass. These sessions thus provide with OCO-2 data points closely collocated with validation targets (over areas that can be as small as 0.2° longitude × 0.2° latitude) and registered over a few minutes (Wunch et al., 2017).

OCO-2 high-resolution spectra are analysed by the ACOS team in order to retrieve X_{CO_2} and other geophysical parameters from them. The ACOS team provides two different X_{CO_2} values: raw and posterior bias-corrected X_{CO_2}. Raw X_{CO_2} is the direct output of the ACOS algorithm following the full physics retrieval: B8 retrospective (B8r) ACOS data release is used here (O'Dell et al., 2018). Posterior bias-corrected X_{CO_2} is an empirically corrected X_{CO_2} that has reduced averaged bias with regard to different "truth-proxies" (O'Dell et al., 2018). In this work, 5AI results are compared with raw X_{CO_2} as we do not perform any empirical bias correction.

250 In addition, we compare X_{CO_2} retrieved from OCO-2 spectra to TCCON data. The TCCON network uses ground-based high resolution Fourier Transform Spectrometers to measure NIR and SWIR spectra that enable the retrieval of the column-averaged dry-air mole fractions of greenhouse gases. These retrievals are performed by GGG2014 (Wunch et al., 2015) and their results are available on the TCCON Data Archive (https://tccondata.org/).

3.2 Data selection

255 We intend to compare 5AI results with regard to TCCON against ACOS results for corresponding sets of soundings. First, we select all the OCO-2 target soundings between 2015 and 2018 with the best ACOS cloud, sounding quality and outcome flags values. As a compromise between scattering particle content and coverage, we set an upper limit of 0.5 for the ACOS retrieved total aerosol optical depth (hereafter denoted AOD). This sample set of OCO-2 target soundings includes 16,414 soundings with a median ACOS retrieved total AOD of 0.05, and a 75% percentile of 0.1.

260

For this study, we select the TCCON official products measured ± 2 hours with regard to OCO-2 overpass time and only keep the target sessions where at least five OCO-2 measurements passing 5AI posterior filters and five TCCON data points are available. This set includes 9,449 TCCON individual retrieval results from 19 TCCON stations listed in Table 2.

Table 2. TCCON data used in this work

TCCON station	Coordinates (latitude, longitude, altitude)	Number of target sessions	Date range (first and last sessions)	Reference
Ascension Island	7.92S, 14.33W, 0.01 km	4	2015-01-16 – 2018-01-15	(Feist et al., 2014)
Bialystok (Poland)	53.23N, 23.03E, 0.18 km	1	2015-03-18	(Deutscher et al., 2019)
Bremen (Germany)	53.10N, 8.85E, 0.027 km	1	2016-03-17	(Notholt et al., 2014)
Caltech (USA)	34.14N, 118.13W, 0.230 km	19	2014-09-12 – 2018-09-16	(Wennberg et al., 2015)
Darwin (Australia)	12.424S, 130.89E, 0.03 km	8	2015-05-15 – 2017-07-28	(Griffith et al., 2014a)
Edwards (USA)	34.96N, 117.88W, 0.700 km	1	2018-08-22	(Iraci et al., 2016)
Eureka (Canada)	80.05N, 86.42W, 0.61 km	2	2015-06-16 – 2015-06-28	(Strong et al., 2019)

Izana (Tenerife)	28.31N, 16.50W, 2.37 km	2	2018-01-05 – 2018-03-24	(Blumenstock et al., 2017)
Karlsruhe (Germany)	49.10N, 8.44E, 0.116 km	1	2016-09-12	(Hase et al., 2015)
Lamont (USA)	36.60N, 97.49W, 0.32 km	9	2015-02-10 – 2016-11-11	(Wennberg et al., 2016)
Lauder (New Zealand)	45.04S, 169.68E, 0.37 km	3	2015-02-17 – 2016-02-06	(Sherlock et al., 2014)
Orléans (France)	47.97N, 2.11E, 0.13 km	1	2015-04-08	(Warneke et al., 2019)
Paris (France)	48.85N, 2.36E, 0.06 km	1	2016-08-25	(Té et al., 2014)
Park Falls (USA)	45.95N, 90.27W, 0.44 km	7	2014-10-11 – 2017-04-21	(Wennberg et al., 2017)
Réunion Island	20.90S, 55.49E, 0.087 km	4	2015-03-24 – 2015-08-01	(De Mazière et al., 2017)
Saga (Japan)	33.24N, 130.29E, 0.007 km	5	2015-07-31 – 2017-12-02	(Kawakami et al., 2014)
Sodankylä (Finland)	67.37N, 26.63E, 0.188 km	4	2015-08-20 – 2018-07-17	(Kivi et al., 2014; Kivi and Heikkinen, 2016)
Tsukuba (Japan)	36.05N, 140.12E, 0.03 km	6	2014-11-14 – 2017-06-17	(Morino et al., 2018)
Wollongong (Australia)	34.40S, 150.88E, 0.03 km	13	2014-09-23 – 2018-05-06	(Griffith et al., 2014b)

265

Besides target data, we also select a sample of OCO-2 nadir land soundings with a coverage as global as possible over the years 2016-2017 (all ACOS flags at their best value possible). For every month and 5° longitude × 5° latitude bins we select 25 (10 for North-America, South-Africa and Australia) soundings with low ACOS retrieved total AOD. For 2016 and 2017, this selection is done for a maximum ACOS retrieved total AOD of 0.035 and 0.045, respectively, yielding 17,069 soundings
270 for 2016 and 11,002 for 2017. Figure 1 shows the spatial and temporal distribution of these OCO-2 points.
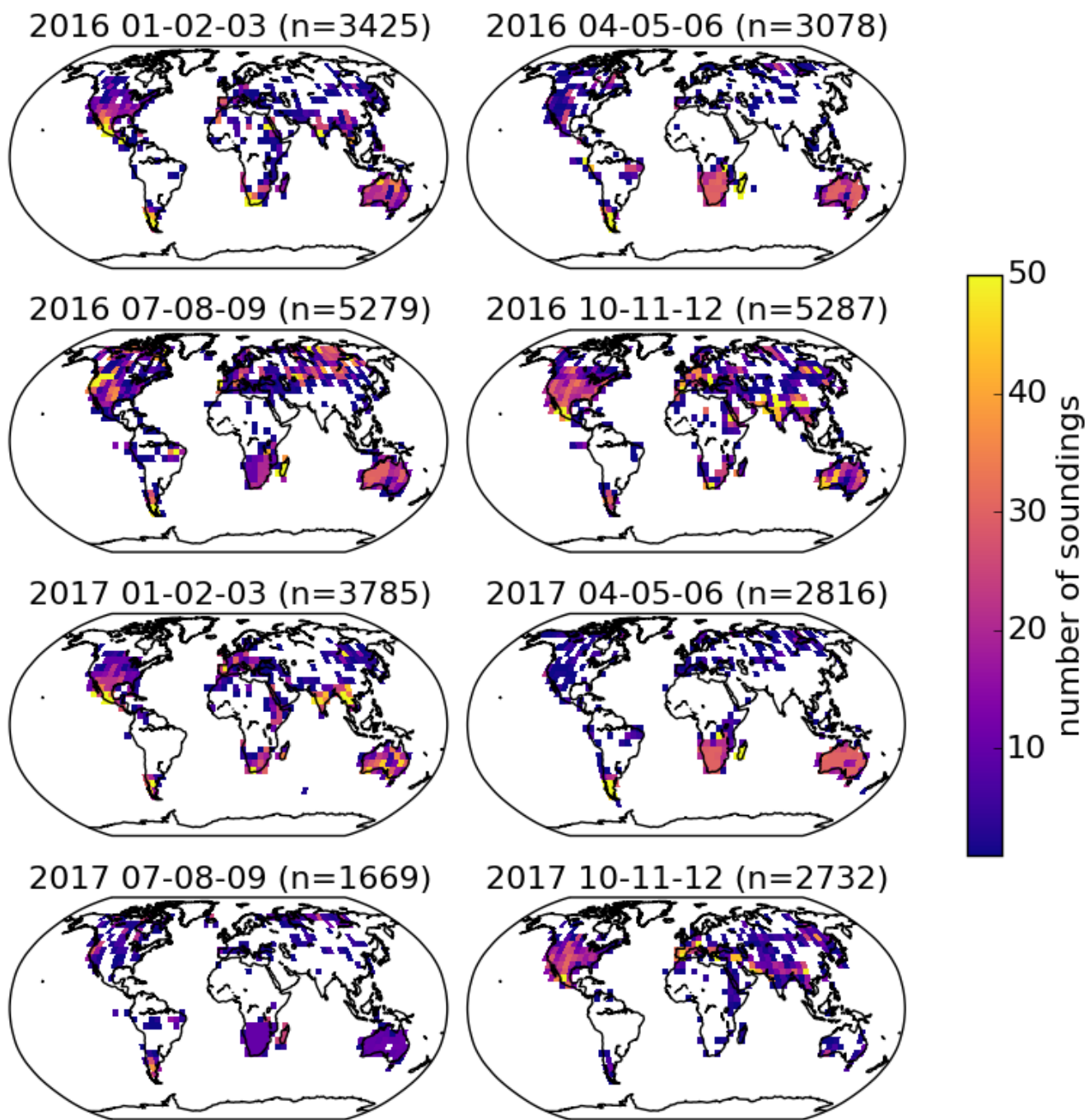
Figure 1. Spatial and temporal repartition of the sample of nadir OCO-2 soundings selected for 5AI retrievals, in seasonal and 5°
× 5° square bins. The titles include the number of soundings n for the corresponding panel: the low number of selected soundings
in July-August-September 2017 is due to an identified OCO-2 data gap.

275

4. Results

4.1 Post-filtering of retrieval results

We apply the a posteriori filters described in Table 3 to ensure retrieval results' quality. The surface pressure filter removes soundings for which it proved difficult to successfully model the optical path, suggesting scattering related errors leading to
280 a large difference between the retrieved and prior surface pressure. The reduced χ^2 filter removes the worst spectral fits. In the end, 95% of our selected soundings pass these first two filters. In addition, the blended albedo filter removes the 12% fraction of target data representative of challenging snow or ice-covered surfaces (Wunch et al., 2011a). With the current retrieval setup, the difference between the 5AI retrieved surface pressure and its prior exhibit an airmass dependence as shown in Fig. 2. For this present work, we filter out all soundings with an airmass above 3.0. Future studies will refine the
285 5AI forward and inverse setup in order to process hyperspectral infrared soundings with larger airmasses. Results detailed in the following subsections are based on the 9,605 target and 21,254 nadir OCO-2 soundings that passed all these filters.

Table 3. Filters applied on 5AI retrieval results for this work.

Variable name	Minimum value	Maximum value	Definition and reference	OCO-2 mode
Retrieved surface pressure	P_{nlev-1}	-	The atmosphere is discretized in 20 levels bounding 19 layers. We do not allow the surface pressure, P_{nlev}, to be lower than its preceding pressure level.	Nadir, Target
Reduced χ^2	-	7.0	Overall goodness of the spectral fit (e.g. Wu et al., 2018)	Nadir, Target
Blended albedo	-	0.8	2.4 x O_2 A-band albedo + 1.13 x CO_2 strong band albedo (Wunch et al., 2011a, 2017)	Target
Airmass	-	3.0	$\frac{1}{\cos(SZA)} + \frac{1}{\cos(VZA)}$, with SZA, the solar zenith angle, and VZA, the viewing zenith angle (Wunch et al., 2011a)	Nadir, Target
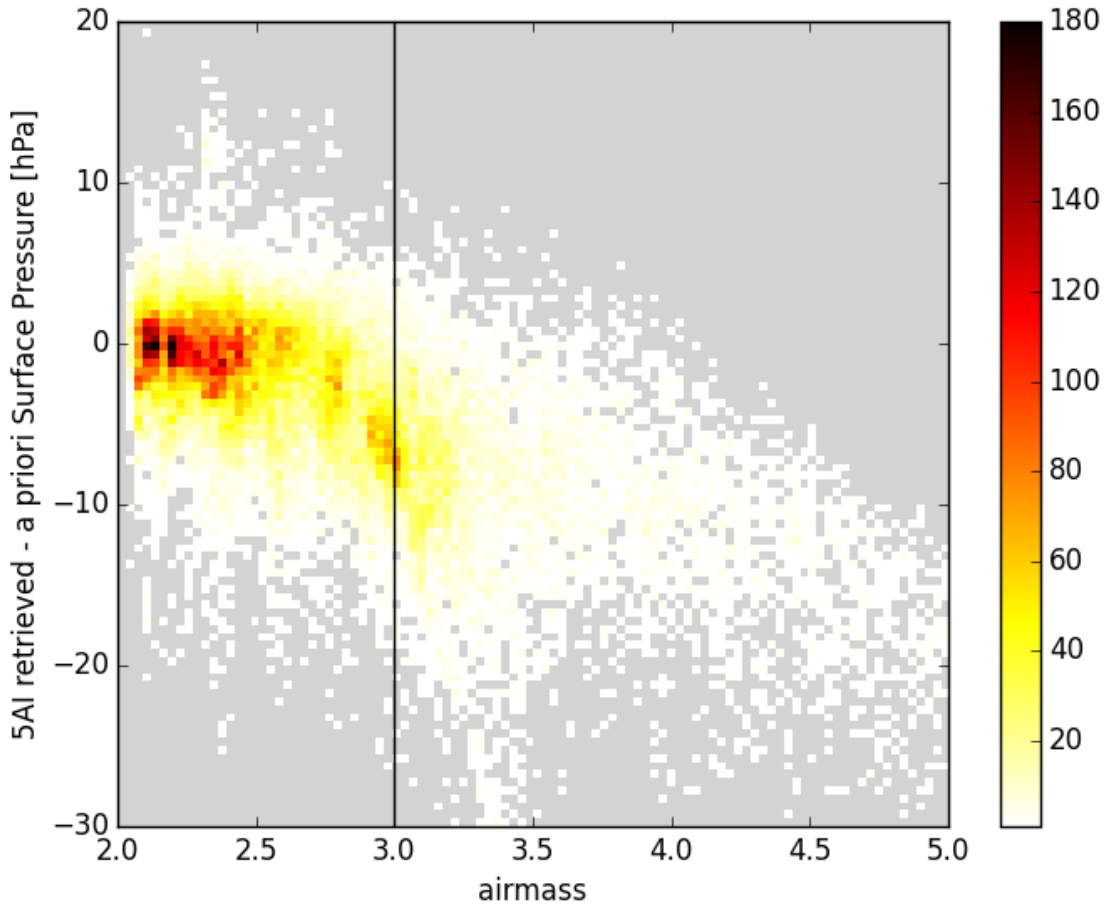
Figure 2. Distribution of target and nadir 5AI retrievals passing surface pressure, blended albedo and reduced χ_r^2 filters according to airmass and difference between retrieved and prior surface pressures. Grey areas denote bins for which no 5AI retrieval is available.

4.2 OCO-2 target retrieval results

For every target session, we consider a unique average of the available retrieval results from OCO-2 measurements and a unique average of the corresponding TCCON official products as performed in e.g. O'Dell et al. (2018) and Wu et al. (2018). As OCO-2 and TCCON X_{CO_2} vertical sensitivities described by their averaging kernels are not exactly identical, we take into account the averaging kernel correction of TCCON data as performed by the ACOS team (O'Dell et al., 2018) and described by Eq. (10) (Nguyen et al., 2014):

$$X_{OCO-2,TCCON} = X_{a\,priori} + (\frac{\hat{X}_{TCCON}}{X_{a\,priori}} - 1) \sum_j \boldsymbol{h}_j (\boldsymbol{a}_{\boldsymbol{CO_2}})_j \boldsymbol{x}_{\boldsymbol{a\,priori,j}} \cdot \tag{10}$$

$X_{OCO-2,TCCON}$ is the column-averaged dry-air mole fraction of CO_2 that would have been retrieved from the OCO-2

300 measurement if the collocated TCCON retrieval was the true state of the atmosphere, $X_{a\,priori}$, the a priori column-averaged

dry-air mole fraction of CO_2, considered to be very similar between 5AI (or ACOS) and GGG2014, $\hat{X}_{TCCON}$, the TCCON

retrieved column-averaged dry-air mole fraction of CO_2, $\boldsymbol{h}$, the pressure weighting function vector defined previously,

$(\boldsymbol{a_{CO_2}})$, the CO_2 column averaging kernel vector defined in Eq. (9) and $\boldsymbol{x_{a\,priori}}$, the a priori CO_2 concentration profile

vector. The effect of this correction yields a positive shift of the bias with regard to TCCON of about 0.2 ppm for the set of

305 target sessions considered in this work.

Following post-filtering, Fig. 3 shows 5AI raw results compared to the TCCON official product over 92 target sessions. The

mean systematic X_{CO_2} bias (5AI $-$ TCCON) is 1.30 ppm and its standard deviation is 1.32 ppm. The ACOS raw X_{CO_2} and

TCCON X_{CO_2} comparison for the corresponding set of OCO-2 soundings is also presented in Fig. 3: the bias with regard to

310 TCCON is -2.28 ppm and its standard deviation is 1.23 ppm. This difference in bias compared to TCCON may be greatly

influenced by forward modelling and retrieval set up differences between 5AI and ACOS, as detailed later in this work.

Bias-corrected FOCAL and RemoTeC X_{CO_2} retrieval results compared to the ACOS official product exhibit similar

differences in bias standard deviations (Reuter et al., 2017b; Wu et al., 2018).
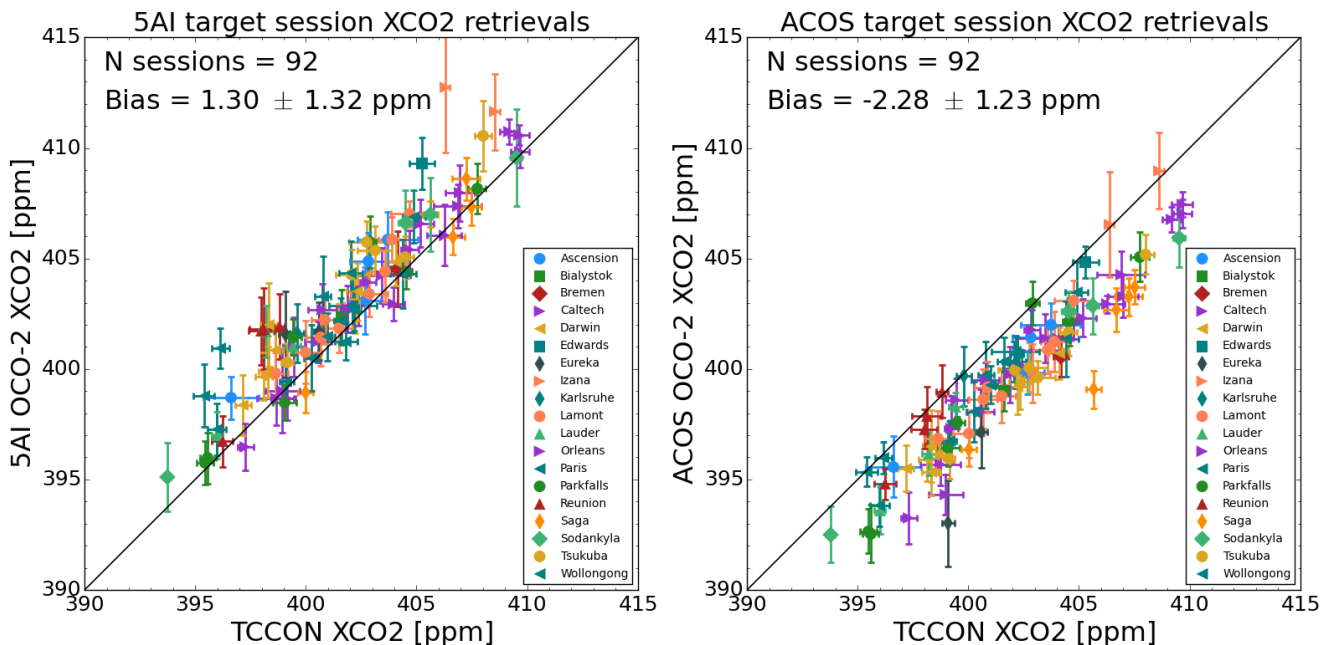
315 **Figure 3. 5AI (left) and raw ACOS B8r (right) OCO-2 target X_{CO_2} retrieval results compared to TCCON official X_{CO_2} product. Individual sounding results are averaged for every target session: markers show session average for OCO-2 and TCCON X_{CO_2}, and error bars show standard deviations.**

Temporal and latitudinal fits of 5AI and ACOS X_{CO_2} biases compared to TCCON are displayed in Fig. 4. Temporal biases are fitted with a 1st order polynomial added to a cosine and exhibit quasi-null slope with a ~0.4 ppm amplitude of yearly oscillation in both 5AI and ACOS cases. Latitudinal bias fits performed with all the available target sessions, except those from Eureka, show that 5AI bias compared to TCCON appears to be larger in the Southern hemisphere than in the Northern hemisphere, but its behaviour is quite parallel to ACOS except at higher latitudes where 5AI and ACOS get closer. The Eureka station (latitude 80°N) has been removed from those fits as satellite retrievals and validation are known to be challenging at these latitudes (O'Dell et al., 2018).
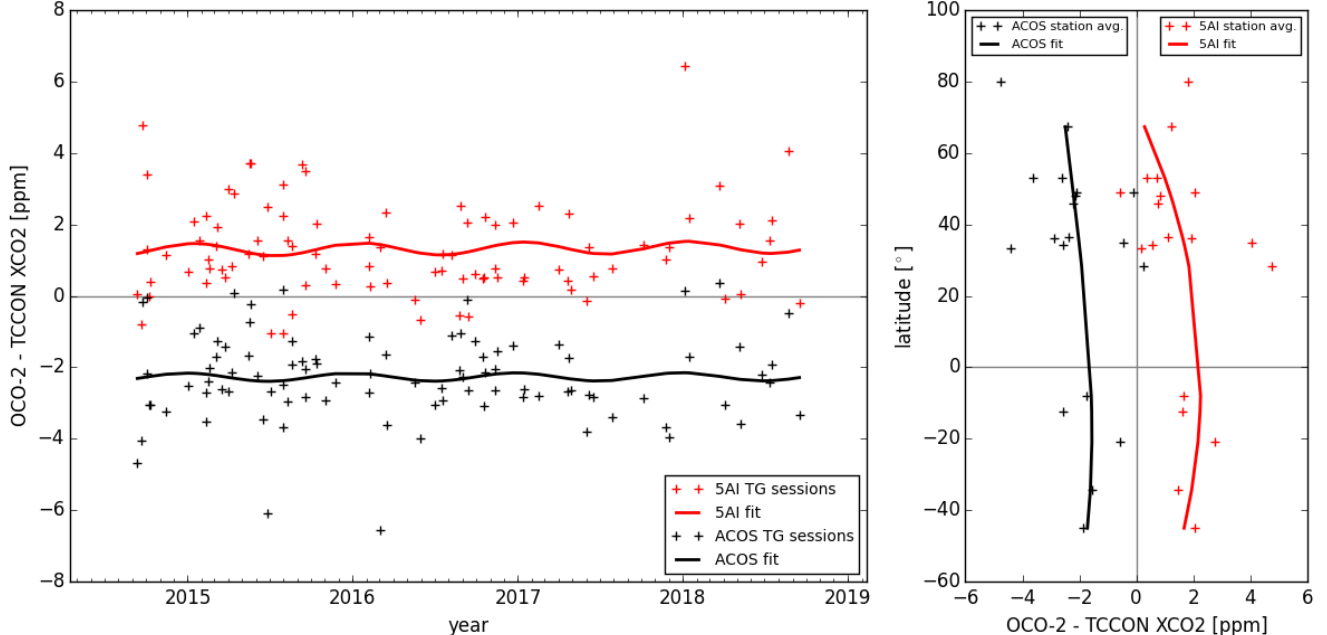
Figure 4. 5AI and raw ACOS B8r OCO-2 target X_{CO_2} bias with regard to TCCON as a function of time (left panel) and latitude (right panel). Crosses show individual session averages in the left panel and individual station averages in the right panel, full lines show polynomial fits of this bias for all target sessions.

4.3 OCO-2 nadir retrieval results

In this subsection, raw 5AI retrieved X_{CO_2} is compared to the ACOS raw product on a sample of OCO-2 nadir soundings as described in Sect. 3 and displayed in Fig. 1. The nadir-viewing configuration is the nominal science mode of the OCO-2 mission and allows comparisons at a larger spatial scale than the one offered by the target mode dedicated to validation.

Figure 5 shows the average and associated standard deviation of the difference between 5AI and ACOS retrieved raw X_{CO_2}. The overall 5AI-ACOS difference is about 3 ppm, with a latitudinal dependency: it is lower above mid-latitudes in the Northern hemisphere. 5AI differences to ACOS also exhibit features over India or the Sahara that are places often associated with strong aerosol events: those may be due to the neglecting of scattering parameters in the 5AI retrievals. The standard

deviation is mainly correlated with topography: it is higher in the vicinity of mountain chains and lower on flatter areas. As we do not take into account topography in the sampling strategy of the processed OCO-2 nadir soundings, its greater

340 variability in mountainous areas can result in a greater variability of the retrieved surface pressure which is strongly correlated with retrieved X_{CO_2}. As for the highest standard deviations in South America, they may be caused by the South Atlantic Anomaly to which they are close (Crisp et al., 2017).
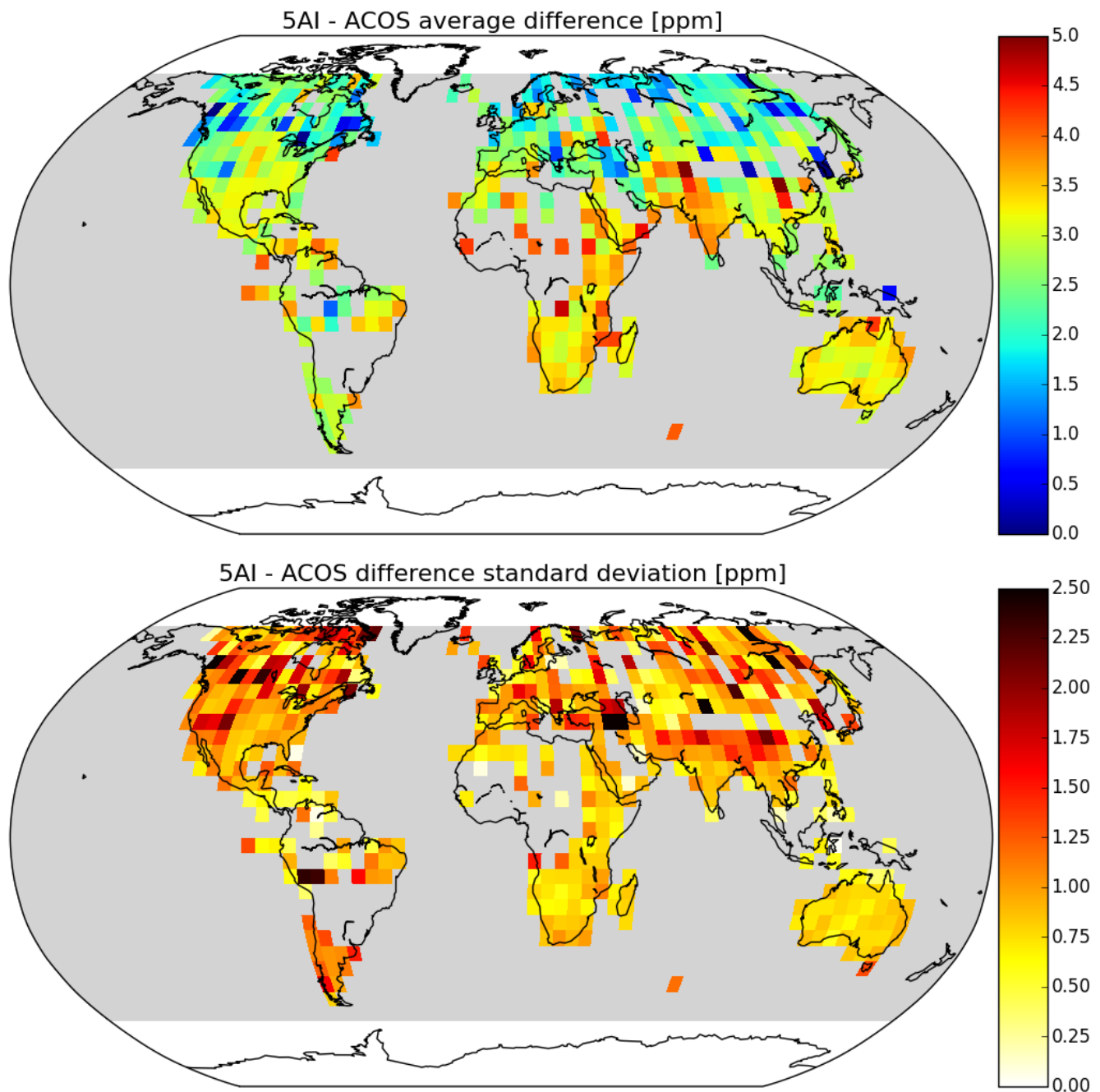
Figure 5. Spatial repartition of 5AI – raw ACOS B8r average difference and its standard deviation on 5° × 5° square bins for the nadir data selection.

As seen in Fig. 6, latitudinal variations of raw 5AI retrieved X_{CO_2} are consistent with those of ACOS, with a difference between the two products almost constant except above mid-latitudes in the Northern hemisphere where the differences are

smaller. In addition, the comparison between 5AI and ACOS in nadir mode is consistent with the results obtained for target

350   sessions. Indeed, the raw 5AI – ACOS target difference lies within $\pm 1\,\sigma$ of nadir results, with σ the standard deviation of

the 5AI – ACOS difference. Figure 7 details the temporal variations of the retrieved X_{CO_2}. The global long-term increase of

the atmospheric concentration of CO_2 can be observed in both hemispheres as well as the seasonal cycle, stronger in the

Northern hemisphere where most of the vegetation respiration and photosynthesis happen. The temporal variations of the

5AI – ACOS X_{CO_2} retrieval differences in nadir mode are also consistent with those presented in target mode.
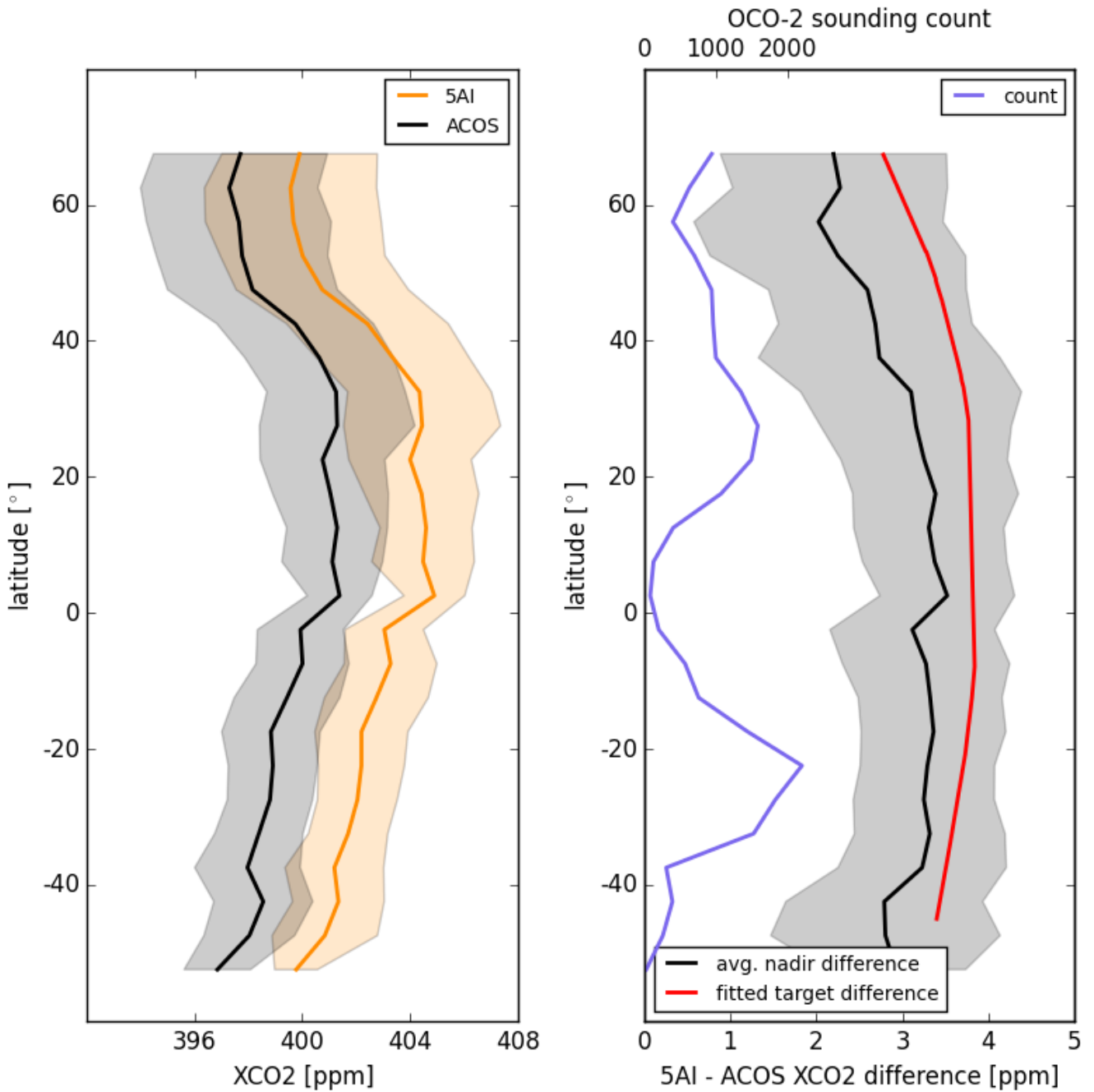
355

Figure 6. Latitudinal variation of 5AI and raw ACOS B8r retrieved X_{CO_2} (left) and their difference (right). The right panel compares 5AI-ACOS average difference for nadir soundings and 5AI-ACOS difference fitted on target sessions (bottom axis). The number of available nadir soundings is also shown in the right panel (top axis).
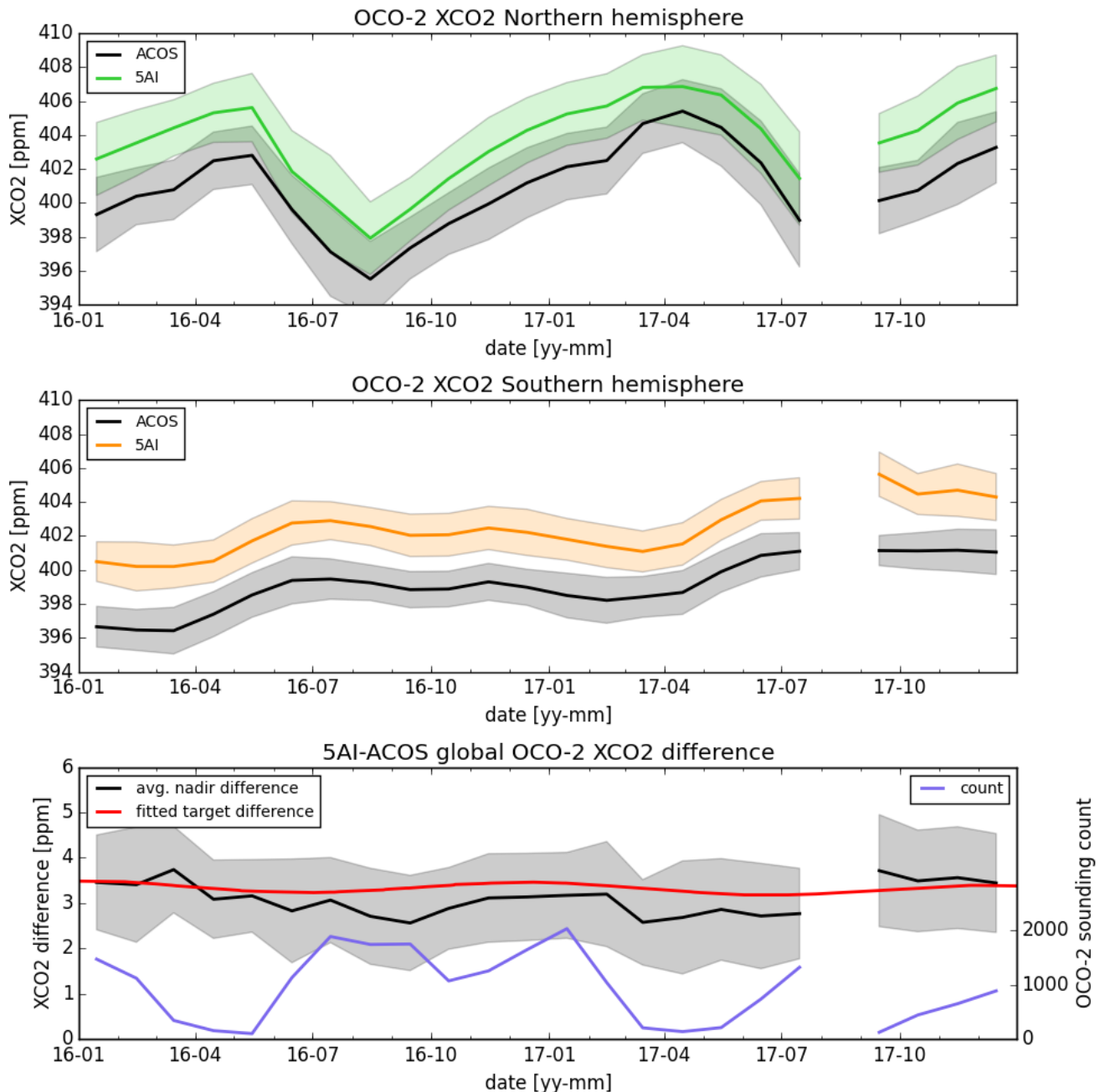
Figure 7. Temporal variation of 5AI and raw ACOS B8r retrieved X_{CO_2} in the Northern hemisphere (top), Southern hemisphere (center) and the global difference (bottom). The bottom panel compares 5AI-ACOS difference for nadir and target OCO-2.

5. Discussion

5.1 Sensitivity of raw retrieval results to scattering particles

One of the main forward and inverse differences between 5AI and ACOS is the accounting of scattering particles on the optical path. Indeed, ACOS considers five Gaussian-shaped vertical profiles of different scattering particle types for which it retrieves three parameters (O'Dell et al., 2018), while, for computational time purposes, none is considered in the previously presented 5AI results (hereafter denoted 5AI-NS for 'no scattering'). In order to assess the sensitivity of 5AI results to this neglecting of scattering particles, we propose here to perform some 5AI X_{CO_2} retrievals from OCO-2 soundings while taking into account some aerosol parameters in the forward modelling and state vector.

Several adaptations of the 5AI setup are required for this sensitivity test (hereafter denoted 5AI-AER for 'aerosols'). First, we consider here two fixed-height fixed-width aerosol layers: the first one representative of coarse mode minerals is located between about 800 and 900 hPa, and the second representative of fine mode soot between about 900 and 1013 hPa. Only the two layer-wise optical depths are retrieved (defined at 755 nm, as ACOS), each with an *a priori* value of 0.025 and an *a priori* uncertainty of 0.15. Otherwise, the state vector and its *a priori* described in Table 1 remain unchanged. Regarding forward modelling, we still rely on 4A/OP coupling with VLIDORT for the O_2 A-band calculations, and we now use 4A/OP coupling with LIDORT for CO_2 weak and strong band calculations (thus still neglecting polarization effects in these bands). Finally, as the retrieval problem becomes less linear when considering scattering particle parameters, we update the Jacobian matrix every iteration.

With these adaptations, 5AI retrievals are about 12 times slower than when not accounting for scattering particles. Considering the increase in computation time, this sensitivity test can only be performed for a small sub-sample of the data. We choose to focus here on 15 OCO-2 target sessions (out of the 92 presented in Sect. 4) that have available AERONET (AErosol RObotic NETwork, version 3: AOD Level 2.0) optical depths ± 2 hours with regard to OCO-2 overpass (Holben et al., 1998; Eck et al., 1999; Giles et al., 2019), thus enabling to also discuss total retrieved aerosol optical depths. A total of 445 OCO-2 soundings have been processed and 228 remain after filtering according to the quality of the spectral fit (reduced $\chi^2 < 7.0$).

Figure 8 shows how taking into account scattering particles in the state vector impacts the retrieval of surface pressure. The airmass dependence exhibited in 5AI-NS results and shown in Fig. 2 appears to be reduced or even removed for the 5AI-AER results. Indeed, neglecting scattering particles results in neglecting the backscattered photons that leads to forward *a priori* synthetic measurements being less intense than those actually measured. This difference is seen by the retrieval scheme as an *a priori* overestimation of the amount of O_2 along the optical, thus as an overestimation of surface pressure which is then reduced. Hence, the -5 hPa surface pressure average bias of 5AI-NS results with regard to the *a priori* surface

395   pressure in Fig. 8, opposed to the 1 hPa bias obtained with 5AI-AER for this small sub-sample of OCO-2 target soundings. Besides, the fraction of measured backscattered photons increases with airmass, leading to the airmass dependence of 5AI-NS results and shown in Fig. 8. Furthermore, adding scattering particle parameters in the retrieval state vector interferes with surface pressure retrieval as scattering particle and surface pressure information carried by the O_2 A-band is entangled. As it can be seen in the right panel of Fig. 8, this leads to lower degrees of freedom for surface pressure compared to retrievals

400   performed without scattering particle parameters in the state vector. 5AI-AER surface pressure degrees of freedom have a distribution way more similar to ACOS' than 5AI-NS surface pressure degrees of freedom. When scattering particle parameters are included in the state vector, this consequently leads to a stronger pull-back of the retrieved surface pressure towards the *a priori*, also helping to reduce or even remove the airmass dependence for surface pressure. Thus, for reasons related to both radiative transfer and the retrieval methodology, taking into account scattering particles modifies the average

405   difference between retrieved and *a priori* surface pressure and helps to remove its airmass dependence seen in 5AI-NS results.
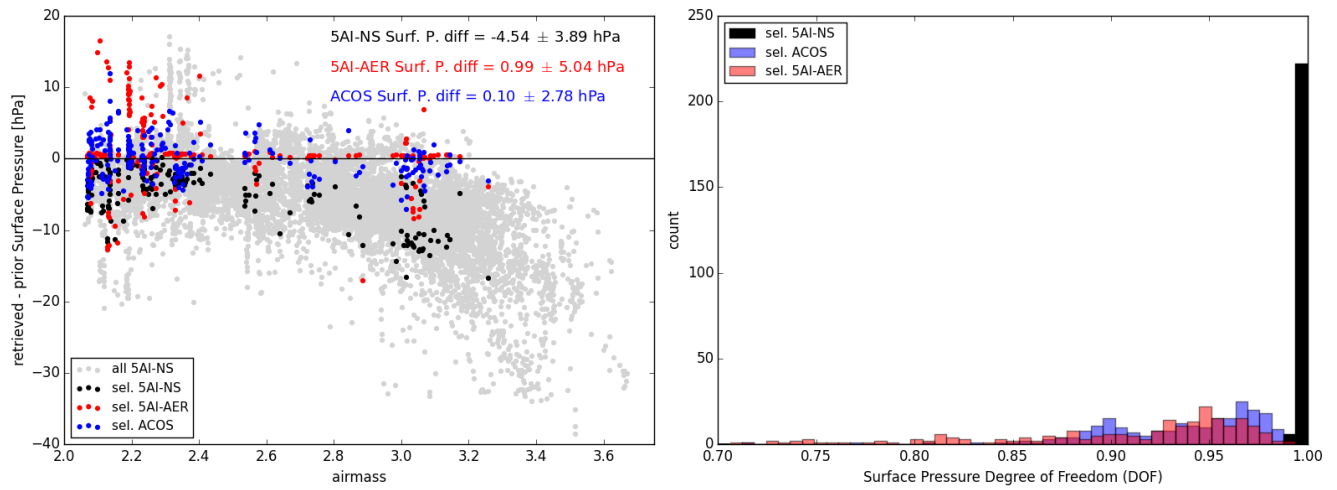
Figure 8. Retrieved surface pressure airmass dependence (left) for all 5AI-NS target OCO-2 soundings (light grey), 5AI-NS soundings selected in the small sub-sample that passed all filters (black), corresponding 5AI-AER (red) and ACOS (blue).
410   **Distributions of surface pressure degrees of freedom (right) for 5AI-NS (black), 5AI-AER (red) and ACOS (blue).**

Figure 9 shows X_{CO_2} retrieved from OCO-2 measurements for these 15 target sessions by (1) the initial 5AI-NS setup (2) this adapted 5AI-AER setup (3) ACOS, in the B8 re-processing raw results. The impact of taking into account scattering particles in the retrievals directly translate from surface pressure to X_{CO_2}: it appears that the difference of about 3 ppm exhibited in

415   5AI-NS results compared to ACOS is reduced to a difference close to 1 ppm in 5AI-AER results. This shows that taking into account scattering particle parameters can indeed explain much of the differences between 5AI-NS results and ACOS. Regarding the retrieved optical depths, Fig.10 shows 5AI-AER and ACOS retrieved total AOD compared to AERONET reference data interpolated at 755 nm. 5AI-AER exhibits a higher average difference to AERONET than ACOS, but both

retrieval algorithms exhibit a considerable scatter of their results compared to AERONET. Efforts to optimize 4A/OP coupling with (V)LIDORT are underway so that more OCO-2 data can be processed. Once those are completed, a dedicated study will help to better tune the 5AI scattering particle setup (varying aerosol types, impact of cirrus clouds, varying layer altitudes, etc).
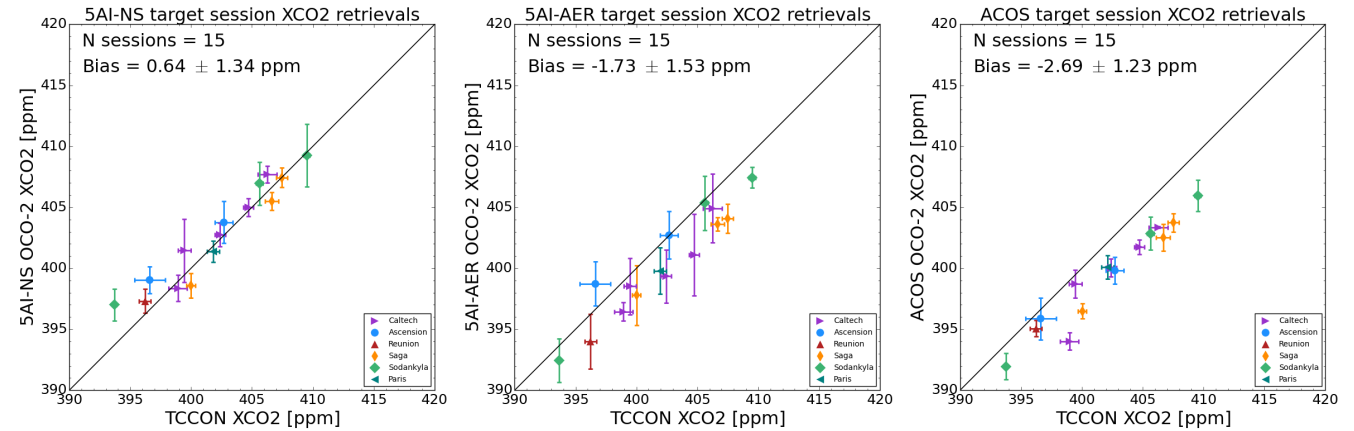
Figure 9. 5AI-NS (left), 5AI-AER (center) and raw ACOS B8r (right) OCO-2 target X_{CO_2} retrieval results compared to TCCON official X_{CO_2} product. Individual sounding results are averaged for every target session: markers show session average for OCO-2 and TCCON X_{CO_2}, and error bars show standard deviations.
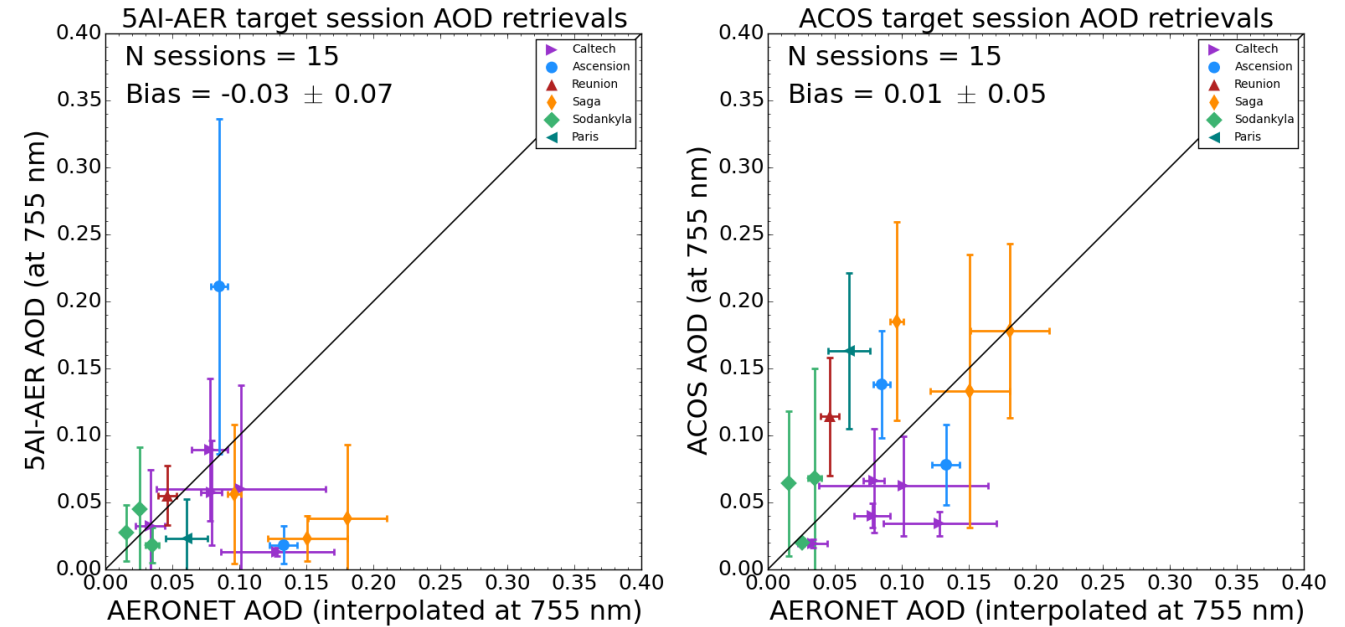
Figure 10. 5AI-AER (left) and ACOS B8r (right) OCO-2 target total AOD retrieval results compared to AERONET AOD interpolated at 755 nm. Individual sounding results are averaged for every target session: markers show session average for OCO-2 and AERONET AOD, and error bars show standard deviations.

5.2 Sensitivity of raw retrieval results to inverse and forward modelling

A difference of about 3 ppm is found between 5AI and ACOS raw X_{CO_2} retrieved from OCO-2 for both nadir and target observations. In Sect. 5.1 we show that neglecting scattering particles for computational time purposes can explain most of this difference. However, the 5AI-AER retrieval setup does not exactly reproduces ACOS setup as state vector, forward radiative transfer and spectroscopic parameter differences remain. All those can be encompassed and accounted for by using an average 'calculated – observed' spectral residual analysis (hereafter 'calc – obs'). It consists in calculating a spectrum (convolved to OCO-2 Instrument Line Shape) based on the ACOS retrieval results (posterior pressure grid, temperature, H_2O and CO_2 profiles as well as albedo and albedo slope) and to compare it to the corresponding OCO-2 observation. Possible background differences are also compensated by scaling the OCO-2 spectrum so that its transparent spectral windows fit those of the calculated 4A/OP spectrum. Such comparisons must be performed and averaged over a spatially and temporally unbiased dataset with a homogenous viewing geometry in order to cancel out possible dependences. Thus, it is here performed for a randomly chosen half of the nadir OCO-2 points with an airmass below 3.0 selected in 2016 (6,790 in total). Figure 11 shows the resulting averaged calculated – observed spectral residuals as well as the corresponding average OCO-2 measurement. Differences are principally located in the 0.7 μm O_2 absorption band, but also in the 1.6 and 2.0 μm CO_2 absorption bands. They are due to the inverse setup and radiative transfer models' differences between ACOS and 5AI (impact of aerosols, parametrization of continua, spectroscopy, etc).
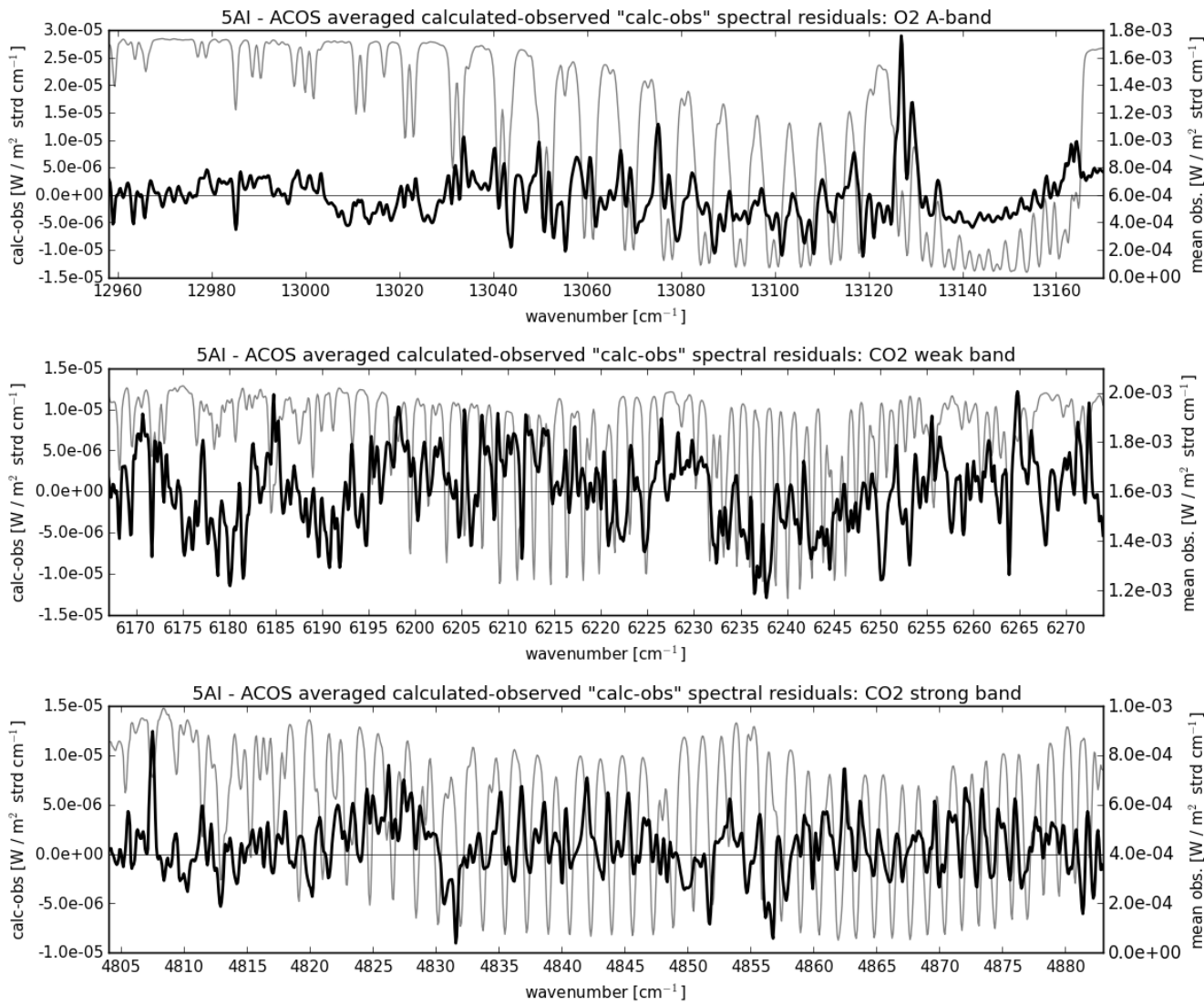
Figure 11. 5AI – ACOS average calculated – observed 'calc-obs' spectral residuals in the O$_2$ A-band (top panel), CO$_2$ weak band (middle panel) and CO$_2$ strong band (bottom panel) appear in thick black lines (left axis). A typical spectrum for the three bands is shown in thin grey lines (right axis).

In order to compare 5AI retrievals with ACOS products while attenuating the impact of the forward and inverse modelling differences, the obtained averaged calc – obs residual is added to every OCO-2 measurements within the complementary half of 2016 selected nadir soundings (6,799 in total). We then apply the 5AI inverse scheme on this new dataset: Fig. 12 compares the distributions of 5AI – ACOS retrieval results obtained with and without the calc – obs adjustment. The systematic differences between 5AI and ACOS results for X_{H_2O}, X_{CO_2}, surface pressure and global temperature profile shift are fully removed when adding the spectral residual adjustment to OCO-2 measurements (remaining differences are negligible compared to standard deviations). This shows that 5AI can on average reproduce ACOS results when all their

respective differences are compensated with a calc – obs adjustment. However, it impacts the standard deviations of 5AI – ACOS differences. Indeed, only ACOS raw results that relate to the 5AI state vector parameters have been used to compute

460   the calculated spectrum used in this calc – obs analysis, and other ACOS parameters, such as scattering particles for instance, have not been considered. Their impact may be attenuated by the background difference correction, which, if disabled, leads to a similar standard deviation of 5AI – ACOS differences in both with and without calc – obs cases. However, without the background compensation, the average difference between 5AI – ACOS is only reduced to 1.9 ppm for X_{CO_2} (not shown). This exemplifies how highly challenging the sounding-to-sounding inter-comparison of retrieval results remains, and

465   highlights how forward modelling and retrieval setup design impact X_{CO_2} retrieval results.
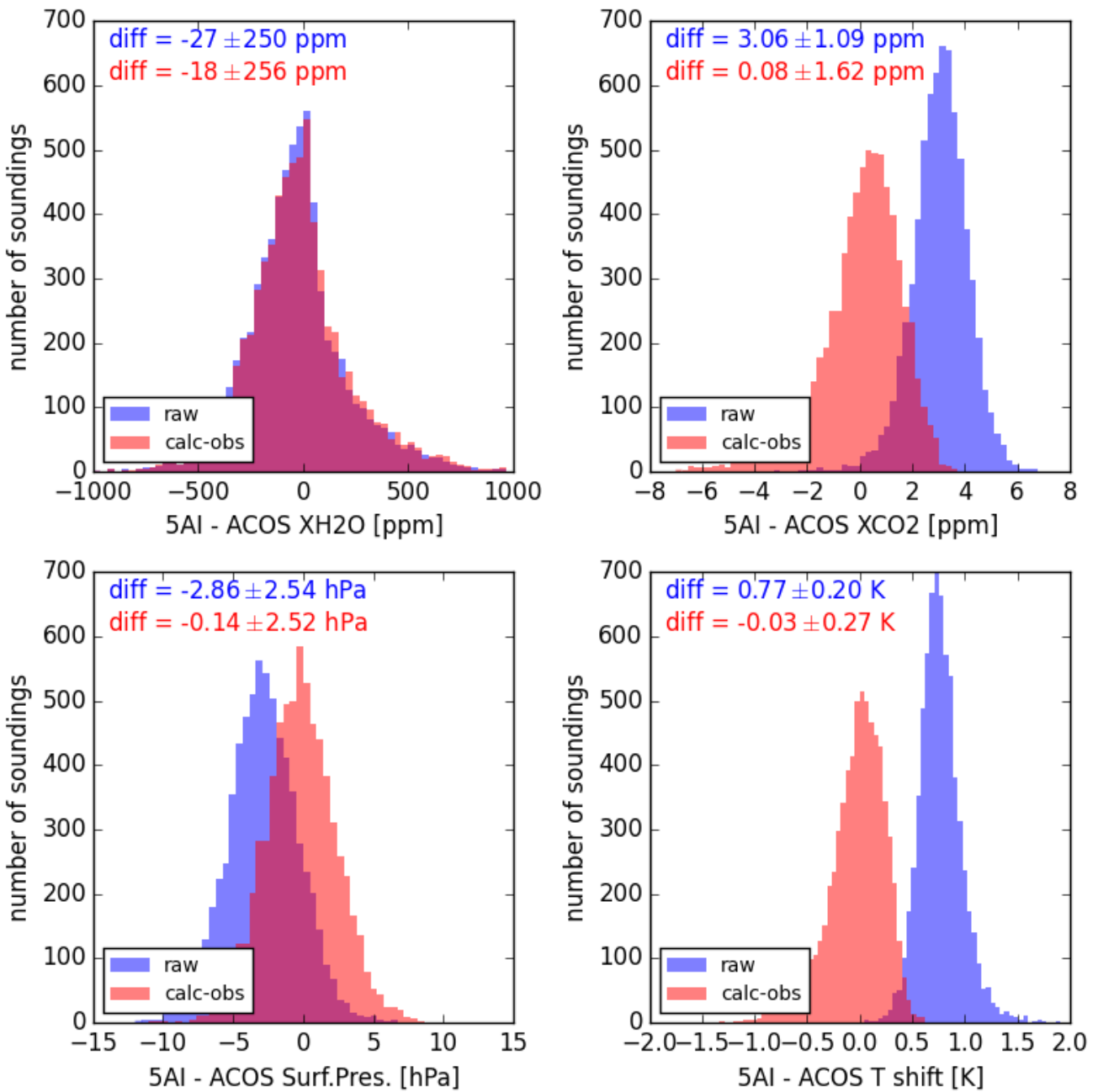
Figure 12. 5AI - raw ACOS B8r difference distributions for X_{H_2O} (top left), X_{CO_2} (top right), surface pressure (bottom left) and temperature profile global shift (bottom right) showed without applying the average calc-obs spectral residual correction (in blue) and with the correction (in red).

6. Conclusions

In this work, we have introduced the 5AI inverse scheme: it implements the Optimal Estimation algorithm and uses the 4A/OP radiative transfer model with the GEISA spectroscopic database and an empirically corrected absorption continuum in the O_2 A-band. We have applied the 5AI inverse scheme to retrieve X_{CO_2} from a sample of ~44k OCO-2 soundings that compromises between coverage and the lowest ACOS retrieved total AOD. We neglected the impact of scattering particles for computation time purposes and obtained a global averaged uncorrected bias with regard to TCCON of 1.30 ppm with a standard deviation of 1.32 ppm, for airmasses below 3.0. These results are comparable in standard deviation with those obtained by ACOS on the corresponding set of OCO-2 soundings. Moreover, we showed that, similarly to ACOS, 5AI X_{CO_2} retrievals satisfactorily capture the global increasing trend of atmospheric CO_2, its seasonal cycle as well as its latitudinal variations, and that 5AI results are consistent between OCO-2 nadir and target modes. Although 5AI exhibits a difference of about 3 ppm with regard to ACOS, we showed that neglecting scattering particles can explain most of it. Indeed, 5AI – ACOS average difference is reduced to 1 ppm when accounting for the optical depths of two coarse and fine mode aerosol layers in 5AI state vector, respectively. This is in part due to how taking into account scattering particles impacts the retrieval of surface pressure, which becomes closer to ACOS. The airmass dependence of the 5AI retrieved surface pressure is also reduced. Finally, we showed that 5AI can on average reproduce ACOS results when adding to OCO-2 measurements an average 'calculated – observed' spectral residual correction. It encompasses all the inverse and forward differences between 5AI and ACOS, and thus underlies the critical sensitivity of retrieval results to the inverse setup design and forward modelling.

For favourable conditions (all best ACOS flags, lowest ACOS retrieved total AOD possible), we showed that 5AI is a reliable implementation of the Optimal Estimation algorithm whose results can be compared to ACOS raw products. Efforts are underway in order to optimize and increase the speed of 4A/OP coupling with (V)LIDORT. Finally, the implementation of the 5AI retrieval scheme is intended to be compatible with 4A/OP structure, so that the code can be easily adapted to any current or future greenhouse gas monitoring instrument, from TCCON or EM27/SUN (e.g. Gisi et al., 2012; Hase et al., 2016) to OCO-2, MicroCarb or CO_2 Monitoring (Meijer and Team, 2019), and even applied to research concepts such as the one proposed in the European Commission H2020 SCARBO project (Brooker, 2018).

Data availability

For this work we use the B8r of OCO-2 data that were produced by the OCO-2 project at the Jet Propulsion Laboratory, California Institute of Technology, and obtained from the OCO-2 data archive maintained at the NASA Goddard Earth Science Data and Information Services Center (NASA GES-DISC). TCCON data are available on the TCCON Data Archive (https://tccondata.org/). AERONET data are available on the AERONET website (https://aeronet.gsfc.nasa.gov/). 5AI

retrieval results presented in this work are available upon request from Matthieu Dogniaux by email (matthieu.dogniaux@lmd.ipsl.fr).

Competing interests

The authors declare that they have no conflict of interest.

505 **Acknowledgements**

This work has received funding from CNES and CNRS. M. Dogniaux is funded by Airbus Defence and Space in the framework of a scientific collaboration with École polytechnique. The authors would like to thank the ACOS team and NASA for OCO-2 data availability. We thank the AERONET team for the whole database availability, and especially Jochen Stutz, Brent Holben, Toshihiko Takemura, Rigel Kivi, Veijo Aaltonen, Francois Ravetta and Jacques Pelon for their
510 effort in establishing and maintaining Caltech, Ascension Island, Réunion St-Denis, Fukuoka, Sodankylä and Paris AERONET sites. Finally, we would like to thank the two anonymous referees whose comments and advice significantly improved the quality of this paper.

The TCCON site at Réunion Island is operated by the Royal Belgian Institute for Space Aeronomy with financial support
515 since 2014 by the EU project ICOS-Inwire and the ministerial decree for ICOS (FR/35/IC1 to FR/35/C5) and local activities supported by LACy/UMR8105 – Université de La Réunion. The TCCON stations at Tsukuba and Burgos are supported in part by the GOSAT series project. Local support for Burgos is provided by the Energy Development Corporation (EDC, Philippines). The Paris TCCON site has received funding from Sorbonne Université, the French research center CNRS, the French space agency CNES, and Région Île-de-France. The Ascension Island TCCON station has been supported by the
520 European Space Agency (ESA) under grant 4000120088/17/I-EF and by the German Bundesministerium für Wirtschaft und Energie (BMWi) under grants 50EE1711C and 50EE1711E. We thank the ESA Ariane Tracking Station at North East Bay, Ascension Island, for hosting and local support. N. Deutscher is funded by ARC Future Fellowship FT180100327. Darwin and Wollongong TCCON stations are supported by ARC grants DP160100598, LE0668470, DP140101552, DP110103118 and DP0879468 and NASA grants NAG5-12247 and NNG05-GD07G.

525 **References**

Basu, S., Guerlet, S., Butz, A., Houweling, S., Hasekamp, O., Aben, I., Krummel, P., Steele, P., Langenfelds, R., Torn, M., Biraud, S., Stephens, B., Andrews, A. and Worthy, D.: Global CO$_{2}$ fluxes estimated from GOSAT retrievals of total column CO$_{2}$, Atmos. Chem. Phys., 13(17), 8695–8717, doi:10.5194/acp-13-8695-2013, 2013.
Basu, S., Baker, D. F., Chevallier, F., Patra, P. K., Liu, J. and Miller, J. B.: The impact of transport model differences on
530 \chem{CO_2} surface flux estimates from OCO-2 retrievals of column average \chem{CO_2}, Atmos. Chem. Phys., 18(10),

7189–7215, doi:10.5194/acp-18-7189-2018, 2018.

Blumenstock, T., Hase, F., Schneider, M., García, O. E. and Sepúlveda, E.: TCCON data from Izana (ES), Release GGG2014.R1, , doi:10.14291/TCCON.GGG2014.IZANA01.R1, 2017.

Bösch, H., Toon, G. C., Sen, B., Washenfelder, R. A., Wennberg, P. O., Buchwitz, M., de Beek, R., Burrows, J. P., Crisp, D., Christi, M., Connor, B. J., Natraj, V. and Yung, Y. L.: Space-based near-infrared CO2 measurements: Testing the Orbiting Carbon Observatory retrieval algorithm and validation concept using SCIAMACHY observations over Park Falls, Wisconsin, J. Geophys. Res. Atmos., 111(D23), doi:10.1029/2006JD007080, 2006.

Bovensmann, H., Burrows, J. P., Buchwitz, M., Frerick, J., Noël, S., Rozanov, V. V., Chance, K. V. and Goede, A. P. H.: SCIAMACHY: Mission objectives and measurement modes, J. Atmos. Sci., 56(2), 127–150, doi:10.1175/1520-0469(1999)056<0127:SMOAMM>2.0.CO;2, 1999.

Brooker, L.: CONSTELLATION OF SMALL SATELLITES FOR THE MONITORING OF GREENHOUSE GASES, in 69th International Astronautical Congress (IAC)., 2018.

Butz, A., Guerlet, S., Hasekamp, O., Schepers, D., Galli, A., Aben, I., Frankenberg, C., Hartmann, J.-M., Tran, H., Kuze, A., Keppel-Aleks, G., Toon, G., Wunch, D., Wennberg, P., Deutscher, N., Griffith, D., Macatangay, R., Messerschmidt, J., Notholt, J. and Warneke, T.: Toward accurate CO2 and CH4 observations from GOSAT, Geophys. Res. Lett., 38(14), doi:10.1029/2011GL047888, 2011.

Chédin, A., Serrar, S., Scott, N. A., Crevoisier, C. and Armante, R.: First global measurement of midtropospheric CO2 from NOAA polar satellites: Tropical zone, J. Geophys. Res. Atmos., 108(D18), doi:10.1029/2003JD003439, 2003.

Cheruy, F., Scott, N. A., Armante, R., Tournier, B. and Chedin, A.: Contribution to the development of radiative transfer models for high spectral resolution observations in the infrared, J. Quant. Spectrosc. Radiat. Transf., 53(6), 597–611, doi:https://doi.org/10.1016/0022-4073(95)00026-H, 1995.

Chevallier, F., Bréon, F.-M. and Rayner, P. J.: Contribution of the Orbiting Carbon Observatory to the estimation of CO2 sources and sinks: Theoretical study in a variational data assimilation framework, J. Geophys. Res. Atmos., 112(D9), doi:10.1029/2006JD007375, 2007.

Connor, B. J., Boesch, H., Toon, G., Sen, B., Miller, C. and Crisp, D.: Orbiting Carbon Observatory: Inverse method and prospective error analysis, J. Geophys. Res. Atmos., 113(D5), doi:10.1029/2006JD008336, 2008.

Crevoisier, C., Heilliette, S., Chédin, A., Serrar, S., Armante, R. and Scott, N. A.: Midtropospheric CO2 concentration retrieval from AIRS observations in the tropics, Geophys. Res. Lett., 31(17), doi:10.1029/2004GL020141, 2004.

Crevoisier, C., Chédin, A., Matsueda, H., Machida, T., Armante, R. and Scott, N. A.: First year of upper tropospheric integrated content of CO$_{2}$ from IASI hyperspectral infrared observations, Atmos. Chem. Phys., 9(14), 4797–4810, doi:10.5194/acp-9-4797-2009, 2009a.

Crevoisier, C., Nobileau, D., Fiore, A. M., Armante, R., Chédin, A. and Scott, N. A.: Tropospheric methane in the tropics – first year from IASI hyperspectral infrared observations, Atmos. Chem. Phys., 9(17), 6337–6350, doi:10.5194/acp-9-6337-2009, 2009b.

Crevoisier, C., Clerbaux, C., Guidard, V., Phulpin, T., Armante, R., Barret, B., Camy-Peyret, C., Chaboureau, J.-P., Coheur, P.-F., Crépeau, L., Dufour, G., Labonnote, L., Lavanant, L., Hadji-Lazaro, J., Herbin, H., Jacquinet-Husson, N., Payan, S., Péquignot, E., Pierangelo, C., Sellitto, P. and Stubenrauch, C.: Towards IASI-New Generation (IASI-NG): impact of improved spectral resolution and radiometric noise on the retrieval of thermodynamic, chemistry and climate variables, Atmos. Meas. Tech., 7(12), 4367–4385, doi:10.5194/amt-7-4367-2014, 2014.

Crisp, D., Pollock, H. R., Rosenberg, R., Chapsky, L., Lee, R. A. M., Oyafuso, F. A., Frankenberg, C., O'Dell, C. W., Bruegge, C. J., Doran, G. B., Eldering, A., Fisher, B. M., Fu, D., Gunson, M. R., Mandrake, L., Osterman, G. B., Schwandner, F. M., Sun, K., Taylor, T. E., Wennberg, P. O. and Wunch, D.: The on-orbit performance of the Orbiting Carbon Observatory-2 (OCO-2) instrument and its radiometrically calibrated products, Atmos. Meas. Tech., 10(1), 59–81, doi:10.5194/amt-10-59-2017, 2017.

Deutscher, N. M., Notholt, J., Messerschmidt, J., Weinzierl, C., Warneke, T., Petri, C. and Grupe, P.: TCCON data from Bialystok (PL), Release GGG2014.R2, , doi:10.14291/TCCON.GGG2014.BIALYSTOK01.R2, 2019.

Drouin, B. J., Benner, D. C., Brown, L. R., Cich, M. J., Crawford, T. J., Devi, V. M., Guillaume, A., Hodges, J. T., Mlawer, E. J., Robichaud, D. J., Oyafuso, F., Payne, V. H., Sung, K., Wishnow, E. H. and Yu, S.: Multispectrum analysis of the oxygen A-band, J. Quant. Spectrosc. Radiat. Transf., 186, 118–138, doi:https://doi.org/10.1016/j.jqsrt.2016.03.037, 2017.

Eck, T. F., Holben, B. N., Reid, J. S., Dubovik, O., Smirnov, A., O'Neill, N. T., Slutsker, I. and Kinne, S.: Wavelength

dependence of the optical depth of biomass burning, urban, and desert dust aerosols, J. Geophys. Res. Atmos., 104(D24), 31333–31349, doi:10.1029/1999JD900923, 1999.

Ehret, G., Bousquet, P., Pierangelo, C., Alpers, M., Millet, B., Abshire, J., Bovensmann, H., Burrows, J., Chevallier, F., Ciais, P. and et al.: MERLIN: A French-German Space Lidar Mission Dedicated to Atmospheric Methane, Remote Sens., 9(10), 1052, doi:10.3390/rs9101052, 2017.

Feist, D. G., Arnold, S. G., John, N. and Geibel, M. C.: TCCON data from Ascension Island (SH), Release GGG2014.R0, , doi:10.14291/TCCON.GGG2014.ASCENSION01.R0/1149285, 2014.

Giles, D. M., Sinyuk, A., Sorokin, M. G., Schafer, J. S., Smirnov, A., Slutsker, I., Eck, T. F., Holben, B. N., Lewis, J. R., Campbell, J. R., Welton, E. J., Korkin, S. V and Lyapustin, A. I.: Advancements in the Aerosol Robotic Network (AERONET) Version~3 database -- automated near-real-time quality control algorithm with improved cloud screening for Sun photometer aerosol optical depth (AOD) measurements, Atmos. Meas. Tech., 12(1), 169–209, doi:10.5194/amt-12-169-2019, 2019.

Gisi, M., Hase, F., Dohe, S., Blumenstock, T., Simon, A. and Keens, A.: XCO$_{2}$-measurements with a tabletop FTS using solar absorption spectroscopy, Atmos. Meas. Tech., 5(11), 2969–2980, doi:10.5194/amt-5-2969-2012, 2012.

Gordon, I. E., Rothman, L. S., Hill, C., Kochanov, R. V, Tan, Y., Bernath, P. F., Birk, M., Boudon, V., Campargue, A., Chance, K. V, Drouin, B. J., Flaud, J.-M., Gamache, R. R., Hodges, J. T., Jacquemart, D., Perevalov, V. I., Perrin, A., Shine, K. P., Smith, M.-A. H., Tennyson, J., Toon, G. C., Tran, H., Tyuterev, V. G., Barbe, A., Császár, A. G., Devi, V. M., Furtenbacher, T., Harrison, J. J., Hartmann, J.-M., Jolly, A., Johnson, T. J., Karman, T., Kleiner, I., Kyuberis, A. A., Loos, J., Lyulin, O. M., Massie, S. T., Mikhailenko, S. N., Moazzen-Ahmadi, N., Müller, H. S. P., Naumenko, O. V, Nikitin, A. V, Polyansky, O. L., Rey, M., Rotger, M., Sharpe, S. W., Sung, K., Starikova, E., Tashkun, S. A., Auwera, J. Vander, Wagner, G., Wilzewski, J., Wcisło, P., Yu, S. and Zak, E. J.: The HITRAN2016 molecular spectroscopic database, J. Quant. Spectrosc. Radiat. Transf., 203, 3–69, doi:https://doi.org/10.1016/j.jqsrt.2017.06.038, 2017.

Griffith, D. W. T., Deutscher, N. M., Velazco, V. A., Wennberg, P. O., Yavin, Y., Keppel-Aleks, G., Washenfelder, R. A., Toon, G. C., Blavier, J.-F., Paton-Walsh, C., Jones, N. B., Kettlewell, G. C., Connor, B. J., Macatangay, R. C., Roehl, C., Ryczek, M., Glowacki, J., Culgan, T. and Bryant, G. W.: TCCON data from Darwin (AU), Release GGG2014.R0, , doi:10.14291/TCCON.GGG2014.DARWIN01.R0/1149290, 2014a.

Griffith, D. W. T., Velazco, V. A., Deutscher, N. M., Paton-Walsh, C., Jones, N. B., Wilson, S. R., Macatangay, R. C., Kettlewell, G. C., Buchholz, R. R. and Riggenbach, M. O.: TCCON data from Wollongong (AU), Release GGG2014.R0, , doi:10.14291/TCCON.GGG2014.WOLLONGONG01.R0/1149291, 2014b.

Hase, F., Blumenstock, T., Dohe, S., Groß, J. and Kiel, M. ä.: TCCON data from Karlsruhe (DE), Release GGG2014.R1, , doi:10.14291/TCCON.GGG2014.KARLSRUHE01.R1/1182416, 2015.

Hase, F., Frey, M., Kiel, M., Blumenstock, T., Harig, R., Keens, A. and Orphal, J.: Addition of a channel for XCO observations to a portable FTIR spectrometer for greenhouse gas measurements, Atmos. Meas. Tech., 9(5), 2303–2313, doi:10.5194/amt-9-2303-2016, 2016.

Holben, B. N., Eck, T. F., Slutsker, I., Tanré, D., Buis, J. P., Setzer, A., Vermote, E., Reagan, J. A., Kaufman, Y. J., Nakajima, T., Lavenu, F., Jankowiak, I. and Smirnov, A.: AERONET—A Federated Instrument Network and Data Archive for Aerosol Characterization, Remote Sens. Environ., 66(1), 1–16, doi:https://doi.org/10.1016/S0034-4257(98)00031-5, 1998.

Houweling, S., Hartmann, W., Aben, I., Schrijver, H., Skidmore, J., Roelofs, G.-J. and Breon, F.-M.: Evidence of systematic errors in SCIAMACHY-observed CO$_{2}$ due to aerosols, Atmos. Chem. Phys., 5(11), 3003–3013, doi:10.5194/acp-5-3003-2005, 2005.

Inoue, M., Morino, I., Uchino, O., Nakatsuru, T., Yoshida, Y., Yokota, T., Wunch, D., Wennberg, P. O., Roehl, C. M., Griffith, D. W. T., Velazco, V. A., Deutscher, N. M., Warneke, T., Notholt, J., Robinson, J., Sherlock, V., Hase, F., Blumenstock, T., Rettinger, M., Sussmann, R., Kyrö, E., Kivi, R., Shiomi, K., Kawakami, S., De Mazière, M., Arnold, S. G., Feist, D. G., Barrow, E. A., Barney, J., Dubey, M., Schneider, M., Iraci, L. T., Podolske, J. R., Hillyard, P. W., Machida, T., Sawa, Y., Tsuboi, K., Matsueda, H., Sweeney, C., Tans, P. P., Andrews, A. E., Biraud, S. C., Fukuyama, Y., Pittman, J. V, Kort, E. A. and Tanaka, T.: Bias corrections of GOSAT SWIR XCO$_{2}$ and XCH$_{4}$ with TCCON data and their evaluation using aircraft measurement data, Atmos. Meas. Tech., 9(8), 3491–3512, doi:10.5194/amt-9-3491-2016, 2016.

Iraci, L. T., Podolske, J. R., Hillyard, P. W., Roehl, C., Wennberg, P. O., Blavier, J.-F., Landeros, J., Allen, N., Wunch, D., Zavaleta, J., Quigley, E., Osterman, G. B., Albertson, R., Dunwoody, K. and Boyden, H.: TCCON data from Edwards (US),

Release GGG2014.R1, , doi:10.14291/TCCON.GGG2014.EDWARDS01.R1/1255068, 2016.

Jacquinet-Husson, N., Armante, R., Scott, N. A., Chédin, A., Crépeau, L., Boutammine, C., Bouhdaoui, A., Crevoisier, C., Capelle, V., Boonne, C., Poulet-Crovisier, N., Barbe, A., Benner], D. [Chris, Boudon, V., Brown, L. R., Buldyreva, J., Campargue, A., Coudert, L. H., Devi, V. M., Down, M. J., Drouin, B. J., Fayt, A., Fittschen, C., Flaud, J.-M., Gamache, R. R., Harrison, J. J., Hill, C., Hodnebrog, Ø., Hu, S.-M., Jacquemart, D., Jolly, A., Jiménez, E., Lavrentieva, N. N., Liu, A.-W., Lodi, L., Lyulin, O. M., Massie, S. T., Mikhailenko, S., Müller, H. S. P., Naumenko, O. V, Nikitin, A., Nielsen, C. J., Orphal, J., Perevalov, V. I., Perrin, A., Polovtseva, E., Predoi-Cross, A., Rotger, M., Ruth, A. A., Yu, S. S., Sung, K., Tashkun, S. A., Tennyson, J., Tyuterev, V. G., Auwera], J. [Vander, Voronin, B. A. and Makie, A.: The 2015 edition of the GEISA spectroscopic database, J. Mol. Spectrosc., 327, 31–72, doi:https://doi.org/10.1016/j.jms.2016.06.007, 2016.

Kawakami, S., Ohyama, H., Arai, K., Okumura, H., Taura, C., Fukamachi, T. and Sakashita, M.: TCCON data from Saga (JP), Release GGG2014.R0, , doi:10.14291/TCCON.GGG2014.SAGA01.R0/1149283, 2014.

Kivi, R. and Heikkinen, P.: Fourier transform spectrometer measurements of column CO_2 at Sodankylä, Finland, Geosci. Instrumentation, Methods Data Syst., 5(2), 271–279, doi:10.5194/gi-5-271-2016, 2016.

Kivi, R., Heikkinen, P. and Kyrö, E.: TCCON data from Sodankylä (FI), Release GGG2014.R0, , doi:10.14291/TCCON.GGG2014.SODANKYLA01.R0/1149280, 2014.

Lamouroux, J., Tran, H., Laraia, A. L., Gamache, R. R., Rothman, L. S., Gordon, I. E. and Hartmann, J.-M.: Updated database plus software for line-mixing in CO2 infrared spectra and their test using laboratory spectra in the 1.5–2.3μm region, J. Quant. Spectrosc. Radiat. Transf., 111(15), 2321–2331, doi:https://doi.org/10.1016/j.jqsrt.2010.03.006, 2010.

De Mazière, M., Sha, M. K., Desmet, F., Hermans, C., Scolas, F., Kumps, N., Metzger, J.-M., Duflot, V. and Cammas, J.-P.: TCCON data from Réunion Island (RE), Release GGG2014.R1, , doi:10.14291/TCCON.GGG2014.REUNION01.R1, 2017.

Meijer, Y. and Team, C.: Copernicus CO2 Monitoring Mission Requirements Document. [online] Available from: https://esamultimedia.esa.int/docs/EarthObservation/CO2M_MRD_v2.0_Issued20190927.pdf, 2019.

Morino, I., Matsuzaki, T. and Horikawa, M.: TCCON data from Tsukuba (JP), 125HR, Release GGG2014.R2, , doi:10.14291/TCCON.GGG2014.TSUKUBA02.R2, 2018.

Nguyen, H., Osterman, G., Wunch, D., O'Dell, C., Mandrake, L., Wennberg, P., Fisher, B. and Castano, R.: A method for colocating satellite X_{CO_2} data to ground-based data and its application to ACOS-GOSAT and TCCON, Atmos. Meas. Tech., 7(8), 2631–2644, doi:10.5194/amt-7-2631-2014, 2014.

Notholt, J., Petri, C., Warneke, T., Deutscher, N. M., Palm, M., Buschmann, M., Weinzierl, C., Macatangay, R. C. and Grupe, P.: TCCON data from Bremen (DE), Release GGG2014.R0, , doi:10.14291/TCCON.GGG2014.BREMEN01.R0/1149275, 2014.

O'Dell, C. W., Connor, B., Bösch, H., O'Brien, D., Frankenberg, C., Castano, R., Christi, M., Eldering, D., Fisher, B., Gunson, M., McDuffie, J., Miller, C. E., Natraj, V., Oyafuso, F., Polonsky, I., Smyth, M., Taylor, T., Toon, G. C., Wennberg, P. O. and Wunch, D.: The ACOS CO_2 retrieval algorithm – Part 1: Description and validation against synthetic observations, Atmos. Meas. Tech., 5(1), 99–121, doi:10.5194/amt-5-99-2012, 2012.

O'Dell, C. W., Eldering, A., Wennberg, P. O., Crisp, D., Gunson, M. R., Fisher, B., Frankenberg, C., Kiel, M., Lindqvist, H., Mandrake, L., Merrelli, A., Natraj, V., Nelson, R. R., Osterman, G. B., Payne, V. H., Taylor, T. E., Wunch, D., Drouin, B. J., Oyafuso, F., Chang, A., McDuffie, J., Smyth, M., Baker, D. F., Basu, S., Chevallier, F., Crowell, S. M. R., Feng, L., Palmer, P. I., Dubey, M., Garc\'\ia, O. E., Griffith, D. W. T., Hase, F., Iraci, L. T., Kivi, R., Morino, I., Notholt, J., Ohyama, H., Petri, C., Roehl, C. M., Sha, M. K., Strong, K., Sussmann, R., Te, Y., Uchino, O. and Velazco, V. A.: Improved retrievals of carbon dioxide from Orbiting Carbon Observatory-2 with the version 8 ACOS algorithm, Atmos. Meas. Tech., 11(12), 6539–6576, doi:10.5194/amt-11-6539-2018, 2018.

Oyafuso, F., Payne, V. H., Drouin, B. J., Devi, V. M., Benner, D. C., Sung, K., Yu, S., Gordon, I. E., Kochanov, R., Tan, Y., Crisp, D., Mlawer, E. J. and Guillaume, A.: High accuracy absorption coefficients for the Orbiting Carbon Observatory-2 (OCO-2) mission: Validation of updated carbon dioxide cross-sections using atmospheric spectra, J. Quant. Spectrosc. Radiat. Transf., 203, 213–223, doi:https://doi.org/10.1016/j.jqsrt.2017.06.012, 2017.

Parker, R., Boesch, H., Cogan, A., Fraser, A., Feng, L., Palmer, P. I., Messerschmidt, J., Deutscher, N., Griffith, D. W. T., Notholt, J., Wennberg, P. O. and Wunch, D.: Methane observations from the Greenhouse Gases Observing SATellite: Comparison to ground-based TCCON data and model calculations, Geophys. Res. Lett., 38(15), doi:10.1029/2011GL047871, 2011.

Pascal, V., Buil, C., Loesel, J., Tauziede, L., Jouglet, D. and Buisson, F.: An improved microcarb dispersive instrumental

concept for the measurement of greenhouse gases concentration in the atmosphere, in International Conference on Space Optics — ICSO 2014, vol. 10563, edited by Z. Sodnik, B. Cugny, and N. Karafolas, pp. 1028–1036, SPIE., 2017.

Le Quéré, C., Raupach, M., Canadell, J., Marland, G., Bopp, L., Ciais, P., Conway, T., Doney, S., Feely, R., Foster, P., Friedlingstein, P., Gurney, K., Houghton, R., House, J., Huntingford, C., Levy, P., Lomas, M., Majkut, J., Metzl, N. and Woodward, I.: Trends in the sources and sinks of carbon dioxide, Nat. Geosci., 2, 831–836, doi:10.1038/ngeo689, 2009.

Rayner, P. J. and O'Brien, D. M.: The utility of remotely sensed CO2 concentration data in surface source inversions, Geophys. Res. Lett., 28(1), 175–178, doi:10.1029/2000GL011912, 2001.

Reuter, M., Bovensmann, H., Buchwitz, M., Burrows, J. P., Connor, B. J., Deutscher, N. M., Griffith, D. W. T., Heymann, J., Keppel-Aleks, G., Messerschmidt, J., Notholt, J., Petri, C., Robinson, J., Schneising, O., Sherlock, V., Velazco, V., Warneke, T., Wennberg, P. O. and Wunch, D.: Retrieval of atmospheric CO2 with enhanced accuracy and precision from SCIAMACHY: Validation with FTS measurements and comparison with model results, J. Geophys. Res. Atmos., 116(D4), doi:10.1029/2010JD015047, 2011.

Reuter, M., Buchwitz, M., Schneising, O., Noël, S., Rozanov, V., Bovensmann, H. and Burrows, J.: A Fast Atmospheric Trace Gas Retrieval for Hyperspectral Instruments Approximating Multiple Scattering—Part 1: Radiative Transfer and a Potential OCO-2 XCO2 Retrieval Setup, Remote Sens., 9(11), 1159, doi:10.3390/rs9111159, 2017a.

Reuter, M., Buchwitz, M., Schneising, O., Noël, S., Bovensmann, H. and Burrows, J.: A Fast Atmospheric Trace Gas Retrieval for Hyperspectral Instruments Approximating Multiple Scattering—Part 2: Application to XCO2 Retrievals from OCO-2, Remote Sens., 9(11), 1102, doi:10.3390/rs9111102, 2017b.

Rodgers, C. D.: Inverse Methods for Atmospheric Sounding, WORLD SCIENTIFIC., 2000.

Scott, N. A. and Chédin, A.: A Fast Line-by-Line Method for Atmospheric Absorption Computations: The Automatized Atmospheric Absorption Atlas, J. Appl. Meteorol., 20(7), 802–812, 1981.

Sherlock, V., Connor, B., Robinson, J., Shiona, H., Smale, D. and Pollard, D. F.: TCCON data from Lauder (NZ), 125HR, Release GGG2014.R0, , doi:10.14291/TCCON.GGG2014.LAUDER02.R0/1149298, 2014.

Spurr, R. J. D.: Simultaneous derivation of intensities and weighting functions in a general pseudo-spherical discrete ordinate radiative transfer treatment, J. Quant. Spectrosc. Radiat. Transf., 75(2), 129–175, doi:https://doi.org/10.1016/S0022-4073(01)00245-X, 2002.

Spurr, R. J. D.: VLIDORT: A linearized pseudo-spherical vector discrete ordinate radiative transfer code for forward model and retrieval studies in multilayer multiple scattering media, J. Quant. Spectrosc. Radiat. Transf., 102(2), 316–342, doi:https://doi.org/10.1016/j.jqsrt.2006.05.005, 2006.

Strong, K., Roche, S., Franklin, J. E., Mendonca, J., Lutsch, E., Weaver, D., Fogal, P. F., Drummond, J. R., Batchelor, R. and Lindenmaier, R.: TCCON data from Eureka (CA), Release GGG2014.R3, , doi:10.14291/TCCON.GGG2014.EUREKA01.R3, 2019.

Té, Y., Jeseck, P. and Janssen, C.: TCCON data from Paris (FR), Release GGG2014.R0, , doi:10.14291/TCCON.GGG2014.PARIS01.R0/1149279, 2014.

Toon, G. C.: Solar Line List for the TCCON 2014 Data Release, , doi:10.14291/TCCON.GGG2014.SOLAR.R0/1221658, 2015.

Tournier: STRANSAC-93 et 4A-93: Développement et validation des nouvelles versions des codes de transfert radiatif pour application au projet IASI, PALAISEAU, France., 1995.

Tran, H. and Hartmann, J.-M.: An improved O2 A band absorption model and its consequences for retrievals of photon paths and surface pressures, J. Geophys. Res. Atmos., 113(D18), doi:10.1029/2008JD010011, 2008.

Warneke, T., Messerschmidt, J., Notholt, J., Weinzierl, C., Deutscher, N. M., Petri, C. and Grupe, P.: TCCON data from Orléans (FR), Release GGG2014.R1, , doi:10.14291/TCCON.GGG2014.ORLEANS01.R1, 2019.

Wennberg, P. O., Wunch, D., Roehl, C. M., Blavier, J.-F., Toon, G. C. and Allen, N. T.: TCCON data from Caltech (US), Release GGG2014.R1, , doi:10.14291/TCCON.GGG2014.PASADENA01.R1/1182415, 2015.

Wennberg, P. O., Wunch, D., Roehl, C. M., Blavier, J.-F., Toon, G. C. and Allen, N. T.: TCCON data from Lamont (US), Release GGG2014.R1, , doi:10.14291/TCCON.GGG2014.LAMONT01.R1/1255070, 2016.

Wennberg, P. O., Roehl, C. M., Wunch, D., Toon, G. C., Blavier, J.-F., Washenfelder, R., Keppel-Aleks, G., Allen, N. T. and Ayers, J.: TCCON data from Park Falls (US), Release GGG2014.R1, , doi:10.14291/TCCON.GGG2014.PARKFALLS01.R1, 2017.

Wu, L., Hasekamp, O., Hu, H., Landgraf, J., Butz, A., aan de Brugh, J., Aben, I., Pollard, D. F., Griffith, D. W. T., Feist, D.

G., Koshelev, D., Hase, F., Toon, G. C., Ohyama, H., Morino, I., Notholt, J., Shiomi, K., Iraci, L., Schneider, M., de Mazière, M., Sussmann, R., Kivi, R., Warneke, T., Goo, T.-Y. and Té, Y.: Carbon dioxide retrieval from OCO-2 satellite observations using the RemoTeC algorithm and validation with TCCON measurements, Atmos. Meas. Tech., 11(5), 3111–3130, doi:10.5194/amt-11-3111-2018, 2018.

735   Wunch, D., Wennberg, P. O., Toon, G. C., Connor, B. J., Fisher, B., Osterman, G. B., Frankenberg, C., Mandrake, L., O'Dell, C., Ahonen, P., Biraud, S. C., Castano, R., Cressie, N., Crisp, D., Deutscher, N. M., Eldering, A., Fisher, M. L., Griffith, D. W. T., Gunson, M., Heikkinen, P., Keppel-Aleks, G., Kyrö, E., Lindenmaier, R., Macatangay, R., Mendonca, J., Messerschmidt, J., Miller, C. E., Morino, I., Notholt, J., Oyafuso, F. A., Rettinger, M., Robinson, J., Roehl, C. M., Salawitch, R. J., Sherlock, V., Strong, K., Sussmann, R., Tanaka, T., Thompson, D. R., Uchino, O., Warneke, T. and Wofsy, S. C.: A

740   method for evaluating bias in global measurements of CO$_{2}$ total columns from space, Atmos. Chem. Phys., 11(23), 12317–12337, doi:10.5194/acp-11-12317-2011, 2011a.

Wunch, D., Toon, G. C., Blavier, J.-F. L., Washenfelder, R. A., Notholt, J., Connor, B. J., Griffith, D. W. T., Sherlock, V. and Wennberg, P. O.: The Total Carbon Column Observing Network, Philos. Trans. R. Soc. A Math. Phys. Eng. Sci., 369(1943), 2087–2112, doi:10.1098/rsta.2010.0240, 2011b.

745   Wunch, D., Toon, G. C., Sherlock, V., Deutscher, N. M., Liu, C., Feist, D. G. and Wennberg, P. O.: The Total Carbon Column Observing Network's GGG2014 Data Version., 2015.

Wunch, D., Wennberg, P. O., Osterman, G., Fisher, B., Naylor, B., Roehl, C. M., O'Dell, C., Mandrake, L., Viatte, C., Kiel, M., Griffith, D. W. T., Deutscher, N. M., Velazco, V. A., Notholt, J., Warneke, T., Petri, C., De Maziere, M., Sha, M. K., Sussmann, R., Rettinger, M., Pollard, D., Robinson, J., Morino, I., Uchino, O., Hase, F., Blumenstock, T., Feist, D. G.,

750   Arnold, S. G., Strong, K., Mendonca, J., Kivi, R., Heikkinen, P., Iraci, L., Podolske, J., Hillyard, P. W., Kawakami, S., Dubey, M. K., Parker, H. A., Sepulveda, E., Garc\'ia, O. E., Te, Y., Jeseck, P., Gunson, M. R., Crisp, D. and Eldering, A.: Comparisons of the Orbiting Carbon Observatory-2 (OCO-2) $X_{\chem{CO_2}}$ measurements with TCCON, Atmos. Meas. Tech., 10(6), 2209–2238, doi:10.5194/amt-10-2209-2017, 2017.

Yokota, T., Yoshida, Y., Eguchi, N., Ota, Y., Tanaka, T., Watanabe, H. and Maksyutov, S.: Global Concentrations of

755   CO_2 and CH_4 Retrieved from GOSAT: First Preliminary Results, SOLA, 5, 160–163, doi:10.2151/sola.2009-041, 2009.

Yoshida, Y., Ota, Y., Eguchi, N., Kikuchi, N., Nobuta, K., Tran, H., Morino, I. and Yokota, T.: Retrieval algorithm for CO$_{2}$ and CH$_{4}$ column abundances from short-wavelength infrared spectral observations by the Greenhouse gases observing satellite, Atmos. Meas. Tech., 4(4), 717–734, doi:10.5194/amt-4-717-2011, 2011.

760   Yoshida, Y., Kikuchi, N., Morino, I., Uchino, O., Oshchepkov, S., Bril, A., Saeki, T., Schutgens, N., Toon, G. C., Wunch, D., Roehl, C. M., Wennberg, P. O., Griffith, D. W. T., Deutscher, N. M., Warneke, T., Notholt, J., Robinson, J., Sherlock, V., Connor, B., Rettinger, M., Sussmann, R., Ahonen, P., Heikkinen, P., Kyrö, E., Mendonca, J., Strong, K., Hase, F., Dohe, S. and Yokota, T.: Improvement of the retrieval algorithm for GOSAT SWIR XCO$_{2}$ and XCH$_{4}$ and their validation using TCCON data, Atmos. Meas. Tech., 6(6), 1533–1547, doi:10.5194/amt-6-1533-2013, 2013.